Product Identification in the Low-Temperature Oxidation of Cyclohexane Using a Jet-Stirred Reactor in Combination with SVUV-PEPICO Analysis and Theoretical Quantum Calculations

Jérémy Bourgalais, Hans-Heinrich Carstensen, Olivier Herbinet, Gustavo A. Garcia, Philippe Arnoux, Luc-Sy Tran, Guillaume Vanhove, Laurent Nahon, Majdi Hochlaf, Frédérique Battin-Leclerc

Published in The Journal of Physical Chemistry A
https://doi.org/10.1021/acs.jpca.2c04490

Product Identification in the Low Temperature Oxidation of Cyclohexane Using a Jet-Stirred Reactor Combined to a SVUV-PEPICO Analysis and Theoretical Quantum Calculations

Jérémy Bourgalais[1,*], Hans-Heinrich Carstensen[2,3], Olivier Herbinet[1], Gustavo A. Garcia[4], Philippe Arnoux[1], Luc-Sy Tran[5], Guillaume Vanhove[5], Laurent Nahon[4], Majdi Hochlaf[6], Frédérique Battin-Leclerc[1]

[1]Université de Lorraine, CNRS, LRGP, F-54000 Nancy, France.
[2]Thermochemical Processes Group (GPT), Department of Chemical and Environmental Engineering, Engineering and Architecture School, University of Zaragoza, Spain
[3]Fundacion Agencia Aragonesa para la Investigacion y el Desarrollo (ARAID), Zagaroza, Spain
[4]Synchrotron SOLEIL, L'Orme des Merisiers, Saint-Aubin-BP 48, 91192 Gif-sur-Yvette Cedex, France
[5]Univ. Lille, CNRS, UMR 8522 – PC2A – Physicochimie des Processus de Combustion et de l'Atmosphère, F-59000 Lille, France
[6]Université Gustave Eiffel, COSYS/LISIS, 5 Bd Descartes 77454, Champs sur Marne, France

* Corresponding author:

J. Bourgalais: jeremy.bourgalais@cnrs.fr

ABSTRACT

Cyclohexane oxidation chemistry was investigated using a near-atmospheric pressure JSR at 570 K and ϕ = 0.8. Numerous intermediates including hydroperoxides and highly oxygenated molecules were detected using synchrotron vacuum ultraviolet photoelectron photoion coincidence spectroscopy. Supported by high-level quantum calculations the analysis of photoelectron spectra allowed the firm identification of molecular species formed during the oxidation of cyclohexane. Besides, this work validates recently published gas chromatography and synchrotron vacuum ultraviolet photoionization mass spectrometry data. Unambiguous detection of characteristic hydroperoxides (e.g. γ-ketohydroperoxides) and their respective decomposition products provide support for the conventional O_2-addition channels up to the third addition and their relative contribution to the cyclohexane oxidation.

The results were also compared to the predictions of a recently proposed new detailed kinetic model of cyclohexane oxidation. Most of the predictions are in line with the current experimental findings highlighting the robustness of the kinetic model. However, the analysis of the recorded slow photoelectron spectra indicating the possible presence of C_5 species in the kinetic model provides hints that substituted cyclopentyl radicals from cyclohexyl ring opening might play a minor role in cyclohexane oxidation. Potentially important missing reaction are discussed.

Graphical abstract

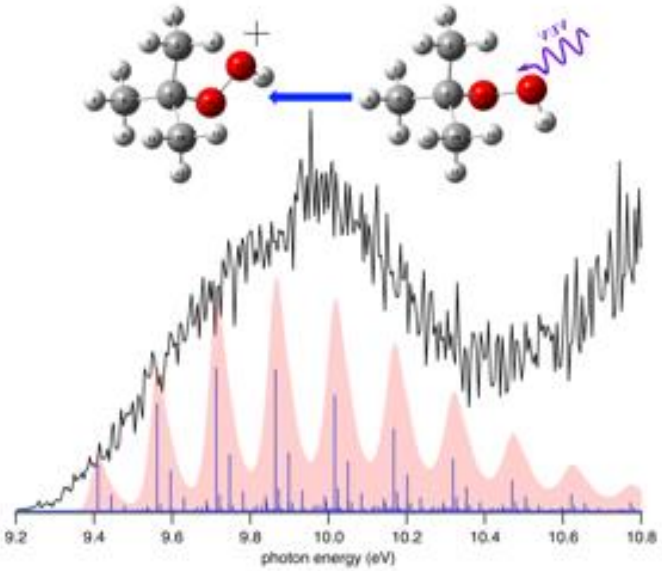

Introduction

The low temperature oxidation (LTO) of hydrocarbons has fascinated researchers for many decades and its overall chemistry is nowadays well-known and broadly accepted especially for acyclic alkanes[1]. Given the strong dependence of ignition behavior on fuel structure, a detailed knowledge of the oxidation behaviors of all fuel components or at least of representative hydrocarbon families is needed to accurately predict the fuel performance in combustion processes. One example is the different reactivity of acyclic and cyclic alkanes. A solid understanding of the LTO chemistry of naphthenes (cycloalkanes and alkylcycloalkanes) would be useful since they constitute a significant part of petroleum-derived transportation fuels[2–4], e.g., ~ 8 wt-% cyclohexane in gasolines, ~ 24 wt-%

alkylcyclohexanes in jet and Diesel fuels[5]. Despite this importance and the availability of numerous studies in the literature, the LTO chemistry of cycloalkanes is still much less understood than that of acyclic alkanes.

Cyclohexane (C_6H_{12}) is a typical cycloalkane adopted in surrogate fuels due to its six-membered saturated carbon ring common to most mono- and multi-alkylated cycloalkanes[6,7]. Containing solely one type of C-H sites, such relatively simple structure of cyclohexane makes it a good candidate for the study of the LTO chemistry of cycloalkanes. Note that the conversion between chair, boat and twisted conformers of cyclohexane is rapid even under LTO conditions (i.e. oxidation below 800 K), which causes equatorial and axial C-H moieties to interconvert and become chemically indistinguishable.

The LTO of cyclohexane has been the subject of several experimental and theoretical investigations and a brief review can be found in the recent work by Zou et al.[8], who reported new experimental data (species profiles measured by photoionization mass spectrometry at Hefei synchrotron and gas chromatograph) starting at 500K and model predictions using a newly developed kinetic mechanism. Zou et al.[8] carried out the LTO of cyclohexane in a jet-stirred reactor (JSR) at 1.04 bar and equivalence ratio ϕ = 0.25. They identified and quantified stable products and reactive intermediates such as hydroperoxides by using both synchrotron vacuum ultraviolet photoionization mass spectrometry (SVUV-PIMS) and gas chromatography coupled to mass spectrometry. With the support of RRKM/master-equation simulations[9], they developed a new kinetic model including for the first time conformational effects of the cyclohexane ring. The most stable conformers of cyclohexane contain H-atoms in axial and equatorial positions. These orientations influence the intramolecular H-transfer channels and subsequent chain reactions in the LTO of cyclohexane. Before the work of Zou et al.[8], only Serinyel et al.[10] proposed a kinetic model, which was validated against cyclohexane LTO data consisting of mole fraction profiles measured by gas chromatography at temperatures below 750 K.

The objective of the present work is to provide new experimental data that allow the identification of products and thus can serve as an additional test for the kinetic model of Zou et al.[8]. Cyclohexane LTO experiments were carried out in a JSR close to atmospheric pressure and under conditions optimized for detecting ketohydroperoxides (KHPs), i.e. with a high contribution of second O_2 addition chemistry. These optimal conditions were searched within the temperature range of T = 560 – 620 K and equivalence ratios between ϕ = 0.5 – 1.0. The optimized experimental conditions in this work are relatively close to those used by Zou et al.[8] and one would expect that the validated kinetic model of Zou et al.[8] to be able to predict the products detected in this current study.

The JSR was coupled to a photoelectron photoion coincidence spectrometer using tunable synchrotron vacuum ultraviolet light for photoionization (SVUV-PEPICO) at the SOLEIL synchrotron (Saint-Aubin, France) to record the mass-selected photoelectron spectra (PES) and total ion yield (TIY) curves of oxidation intermediates and products. PES contain isomer-specific information, which allows the identifications of species of a given m/z ratio through comparison with experimental reference spectra taken from the literature or through theoretical spectra from high-level theoretical quantum calculations performed within this study. Readers may refer to Hemberger et al.[11] for a recent review of the application of this advanced diagnostic tool in combustion research. In principle, SVUV-PEPICO is more suitable than the SVUV-PIMS method used by Zou et al.[8] for species identification and especially isomer discrimination because the structure of SVUV-PEPICO spectra reflects the isomer-specific vibronic transitions of the photoionization step.

The paper is organized as follows. First, the experimental setup and the theoretical calculations performed to support the experimental data analysis are described, as well as the kinetic model from the literature[8] used to simulate the LTO of cyclohexane. Second, an overview spectrum of the LTO of cyclohexane and tests for condition optimizations are presented. The following part provides an overview of the species identified in this study at 570 K and ϕ=0.8 and compares those to the species detected in the two most recent LTO experimental studies (Serinyel et al.[10] and Zou et al.[8]) and to the species predicted by the kinetic model of Zou et al.[8]. Finally, in the last part, the PES and TIY of the most important species are analyzed and compared to the predictions of the most important reaction pathways leading to products and intermediates. Additional spectra for less important species are provided in the supplementary material (SM). For cases in which the kinetic model fails to predict observed molecules, possibly missing pathways are discussed at the end of the result section and a conclusion summarizes the information of the results part at the end of the manuscript.

Experimental and theoretical methods

Experimental procedure

The experiments were performed on the VUV DESIRS beamline at the SOLEIL synchrotron. The experimental setup is identical to that described in Bourgalais et al.[12,13] and Battin-Leclerc et al.[14] and only a summary with the specificities related to this work is given here.

A lean reactive gas mixture (cyclohexane + O_2 + He) was continuously flowed into a JSR ($\sim 60\ \mathrm{cm}^3$) maintained near atmospheric pressure (1.07 bar). The purity of the gases used for the experiments is 99.9% for the fuel and 99.999% for both O_2 and He. The liquid cyclohexane fuel was mixed homogeneously into the gas flow and evaporated using a controlled evaporator mixer (CEM) upstream of the JSR and He as a carrier gas. Each experiment was performed at a constant temperature and inlet flow rates were adjusted at each temperature between 560 and 620 K to set a specific equivalence ratio (ϕ=0.5-1.0) and residence time ($\tau = 3s$). The inlet mole fraction of the fuel was set to 0.01.

The heated JSR was mounted inside the SAPHIRS chamber permanent end-station[15], located at one of the monochromatized branches of the VUV DESIRS beamline. At one extremity of the JSR, a 100 µm orifice creates a molecular beam in the vacuum chamber. The molecular beam passes through two consecutive skimmers expanding further towards the ionization chamber where it crosses the focused VUV synchrotron light. Then, the double-imaging photoelectron/photoion (i^{2}PEPICO) spectrometer DELICIOUS III detects the electrons and cations in coincidence[16]. The photoionization mass spectra are recorded with a typical mass resolution ~1,700 (FWHM). Photoelectrons images are then sorted by associated cation mass and treated with an Abel transform algorithm to extract the PES. There are two modes for obtaining the cation spectroscopy via the PES depending on the resolution vs acquisition time compromise:

(1) A velocity map imaging PES (VMI-PES) can be recorded at a fixed photon energy by plotting the photoelectron count as a function of binding energy (photon – electron kinetic energy), allowing for shorter acquisition time but lower resolution[17].
(2) The coincidence signal can be plotted as a function of photoelectron count and photon energy, from which a slow photoelectron spectrum (SPES) can be obtained by integration of the photoelectron signal with near-zero kinetic energy[18]. The SPES

have been corrected by the beamline's flux as measured with a dedicated photodiode. Here, the total (photon + electron) energy resolution of the SPES is ~20 meV.

A complementary analysis of the oxidation products can also be done using mass-selected total ion yield (TIY) curves in the case of low signal-to-noise ratio preventing PES analysis. TIY curves are obtained by considering all coincidence events, independent of the photoelectron kinetic energy, and are proportional to the photoionization cross section of a given species.

Theoretical calculations

Energy-minimized structural conformations of all valid structures were first selected using Global-MMX which is a steric energy minimization program to search for the global energy minimum and other low energy local minima. The conformers were then used as starting structures for hybrid B3LYP density functional theory (DFT) calculations to find the lowest energy structures[19]. Optimized geometries were calculated at the B3LYP/6-31G* level of theory. The geometries of the lowest energy conformers were reoptimized along with frequency calculations at the PBE0/aug-cc-pVDZ level[20–22]. The optimized geometry of the neutral species was used as initial guess in the optimization of the cation structure. The frequencies at the PBE0/aug-cc-pVDZ level were also used to calculate the zero-point energy (ZPE) correction to the ionization energies (see below). A Franck Condon (FC) analysis was performed to simulate the vibrationally-resolved electronic spectra at 0 K by means of the Time-Independent Adiabatic Hessian Franck–Condon (TI-AH|FC) model[23–26]. The resulting stick spectrum has been convolved with a 20 meV bandwidth Gaussian profile to account for the resolution of the experimental SPES. When available, a comparison between experimental reference and simulated spectra is presented to benchmark the theoretical methodology.

For the determination of the adiabatic ionization energy (AIE), the CBS-QB3 zero-point vibrational energy (ZPE)-corrected total electronic energies for the neutral and cation ground states were used in the first place[27,28]. When further clarifications were required, single point computations were carried out on the optimized structures using the explicitly correlated coupled cluster with single, double and perturbative triple excitations ((R)CCSD(T)-F12)[29–32]. This was used together with the aug-cc-pVDZ basis set in conjunction with the corresponding resolutions of the identity and density fitting functions[33] as generated by MOLPRO[34]. Finally, the computed spectra at the (R)CCSD(T)-F12/aug-cc-pVDZ(SP)// PBE0/aug-cc-pVDZ level of theory were shifted manually in energy to improve agreement with the experimental spectra.

Kinetic model

The experimental spectra measured at the SOLEIL synchrotron are compared to simulations performed using the kinetic model from Zou et al.[8] and the openSMOKE++ software package[35,36] using the JSR module. Briefly, the reaction scheme from the kinetic model of Zou et al.[8] is an update of a kinetic model on the LTO of ethylcyclohexane[37] including conformational effects. The base mechanism comes from a model on propene oxidation of Burke et al.[38] and the construction of the cyclohexane sub-mechanism for the first and second dioxygen additions is based on theoretical calculations of Zou et al.[9]. The thermodynamic data of the species were either taken from Silke et al.[39] or calculated with the THERGAS code[40].

Overall description of the experimental results

After presenting the obtained mass spectrum, this part describes how the optimized conditions were obtained and then lists all the molecular species, which were identified during this work.

Cyclohexane LTO Overview Spectrum

Figure 1 shows the mass spectrum recorded during the LTO of cyclohexane at the conditions ϕ = 0.5 and T = 590 K. The scan ranged from 25 amu to 165 amu. The highest mass detected at these conditions is m/z 144 and the lowest one m/z 28. The largest signal corresponds to the cyclohexane parent, clearly identified at m/z 84 through comparison to the PES by Ikuta et al.[41] (see Figure S1 in SM). The spectrum in Figure 1 shows that decomposition products (< 6 carbons) and oxidized products (6 carbon atoms with one or more oxygen atoms) are detected with good signal-to-noise ratio. Only the signal of the highest oxidized product ($C_6H_8O_4$) is weak, although still clearly visible. Signals of molecules with more than 5 oxygen atoms are missing. Based on this initial spectrum, the signal strength of highly oxidized products was optimized.

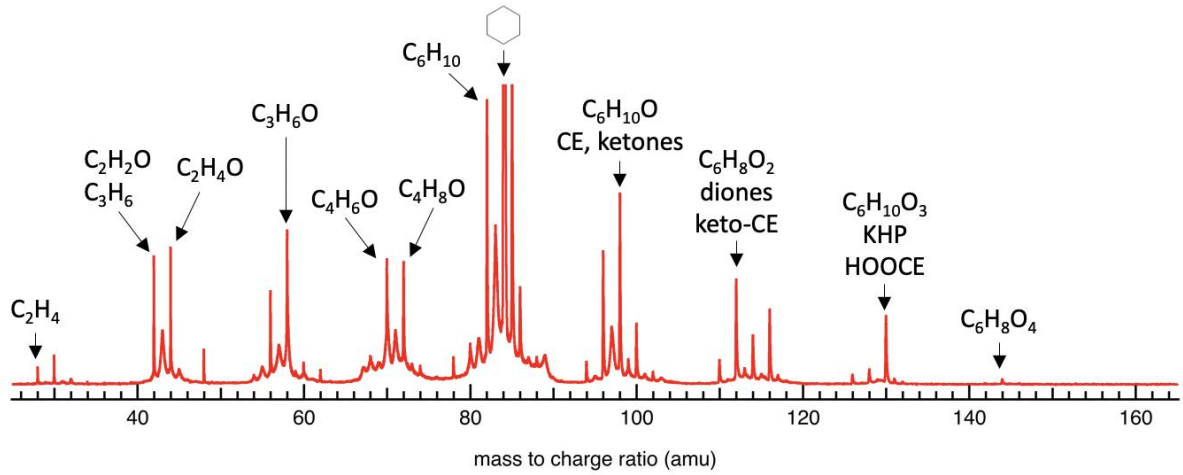

Figure 1: Typical time-of-flight mass spectrum obtained by integration over the photon energy range from 10.0 to 11.0 eV with a step size of 5 meV and an acquisition time of 80 s per step during the LTO of cyclohexane at ϕ = 0.5 and T = 590 K. The vertical scale is reduced to zoom out the low intensity peaks so that cyclohexane (m/z 84) and its 7% ^{13}C isotopomer (m/z 85) are cut off.

Determination of optimized conditions for detailed species analysis

The equivalence ratio and the temperature were varied to find the best conditions for the detection of oxidation products such as KHPs that play a key role in the LTO of alkanes[42,43]. The temperature was varied from 560 to 620 K and the equivalence ratio between 0.5 and 1.0. In Figure 2, the impact of temperature on fuel consumption (left) and on the yields of 2- and 3-oxygen atom containing products (m/z 116 and 130 respectively) are shown. In the left part of Figure 2, the experimental signal at m/z 84 is shifted to fit the temperature evolution of the mole fraction of cyclohexane simulated using the model of Zou et al.[7]. Both shapes agree relatively well. Based on the modelling results, one can see that around 600 K more than 60% of cyclohexane is consumed. Raising the temperature beyond 600 K has no (in the experimental data) or just a small (in the simulations) effect on the degree of cyclohexane

consumption. Indeed this temperature region marks the beginning of the negative temperature coefficient (NTC) zone[10]. A quick mass spectrum at 10 eV, provided in the SM (Figure S2), shows that cyclohexane starts to be already consumed at 560 K because signals for m/z 83 (fragment of cyclohexyl or its isomers) and m/z 82 (presumably cyclohexene or its isomers) are clearly detected.

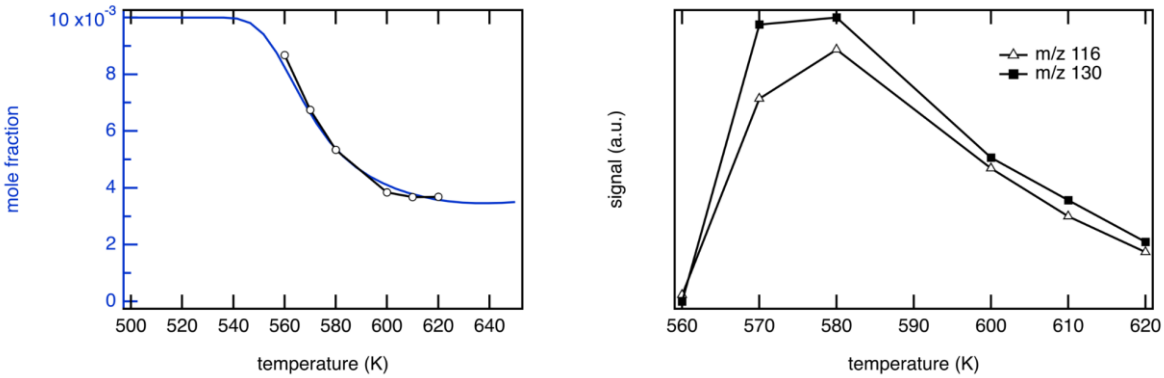

Figure 2: Optimization of KHP detection. Left: Comparison of the mole fraction of cyclohexane predicted using the kinetic model of Zou et al.[8] (blue line) and the integrated area of signal of m/z 84 measured at a fixed photon energy of 10.0 eV for ϕ = 0.5 during the LTO of cyclohexane (open circles). Right: Signal of m/z 116 (open triangles) and 130 (black squares) at a fixed photon energy of 10.0 eV during the LTO of cyclohexane as a function of the temperature at ϕ = 0.5.

The right part of Figure 2 shows how the signals of m/z 116 and 130, which belong to partially oxidized intermediates of cyclohexane LTO vary with temperature. These profiles clearly differ from that of cyclohexane conversion and indicate that 570 - 580 K is an optimal temperature region to study these oxidized products. Based on similar tests with varying equivalence ratios ϕ (Figure S3) and the fact that a weak signal at m/z 162 appeared (Figure S4), the configuration T = 570 K, ϕ = 0.8 was selected for a detailed analysis of the cyclohexane LTO products. Note that Zou et al.[8] observed in their JSR experiments that the signal for most hydroperoxides reached peak values at 575 K, which emphasizes the similarity of both sets of experimental data. The results of the current cyclohexane LTO study are presented in the following sections.

Summary of species identified in the LTO of cyclohexane

A summary of the m/z peaks detected in this study together with the species assignments based on their associated photoelectron spectra is given in Table 1. This table also provides a guide to the figures that show the corresponding PES or TIY curves. The results are compared to the studies by Serinyel et al.[10] and Zou et al.[8] under comparable conditions.

Table 1: Summary of species identified and discussed in this study using the PEPICO technique at 570 K and ϕ = 0.8 and those by Serinyel et al.[10] and by Zou et al.[8]

m/z	Formula	Species detected by PEPICO	Degree of confidence in identification[a]	Figure	Previous experimental detections	
					Serinyel et al.[b,d]	Zou et al.[c,d]
28	C_2H_4	ethene	***	S5	X	X
34	H_2O_2	hydrogen peroxide	***	S6	–	X

42	C_2H_2O	ketene	***	S7	–	X
	C_3H_6	propene	***		X	–
44	C_2H_4O	acetaldehyde	***	S8	X	X
		ethenol	**		–	X
		oxirane	***		X	–
46	CH_2O_2	formic acid	***	S24	–	X
48	CH_4O_2	methyl hydroperoxide	***	S11	–	X
54	C_4H_6	buta-1,3-diene	***	S21	X	X
56	C_3H_4O	prop-2-enal	***	S9	X	X
	C_4H_8	but-1-ene	?		X	–
60	$C_2H_4O_2$	acetic acid	***	S10	–	X
	C_3H_8O	methoxyethane	**		–	–
62	$C_2H_6O_2$	ethyl hydroperoxide	***	S12	–	X
70	C_4H_6O	but-3-en-2-one	***	S22	–	–
		2-methylprop-2-enal	***		–	–
		but-3-enal	***		–	X
72	C_4H_8O	oxolane	**	S23	–	X
		butanal	***		–	X
		2,2-dimethyloxirane	***		–	–
	$C_3H_4O_2$	propanedial	***		–	X
74	$C_3H_6O_2$	allyl hydroperoxide	***	S13	–	D
78	C_6H_6	benzene	***	S18	X	D
		fulvene	?		–	
		1,2-hexadiene-5-yne	*		-	-
80	C_6H_8	cyclohexa-1,3-diene	**	S17	–	D
		cyclohexa-1,4-diene	**		–	
	C_5H_4O	cyclopenta-2,4-dien-1-one	**		–	
82	C_6H_{10}	cyclohexene	***	Figure 4	X	X
		methylidenecyclopentane	?		–	–
84	C_6H_{12}	cyclohexane	***	S1	X	X
	C_5H_8O	pent-4-en-2-one	?		–	X
88	$C_4H_8O_2$	butenyl hydroperoxide	***	S14	–	D
94	C_6H_6O	phenol	**	S19	X	D
96	C_6H_8O	cyclohex-2-en-1-one	***	S20	X	D
98	$C_6H_{10}O$	cyclohexanone	***	Figure 7	X	X
		hex-5-enal	?		X	X
		1,2-epoxycyclohexane	***		X	X
		1,4-epoxycyclohexane	**		X	X
		cyclopentanecarbaldehyde	?		X	–
100	$C_6H_{12}O$	cyclohexanol	?	Figure 8	X	D
	$C_5H_8O_2$	3-hydroperoxycyclopentene	**		–	–
		4-hydroperoxycyclopentene	**		–	–
112	$C_6H_8O_2$	cyclohexane-1,2-dione	*	Figure 12	–	–
		4-oxohex-5-enal	**		–	–
		cyclohexane-1,3-dione	**		–	X
		3-oxohex-5-enal	**		–	X
		cyclohexane-1,4-dione	*		–	–
114	$C_6H_{10}O_2$	hexanedial	?	Figure 13	–	X
		3-hydroperoxy cyclohexene	***		–	X
		4-hydroperoxy cyclohexene	***		–	X
116	$C_6H_{12}O_2$	hydroperoxycyclohexane	?	Figure 5	–	x
	$C_5H_8O_3$	3,5-epoxy-cyclopentyl hydroperoxide	***		–	–
126	$C_6H_6O_3$	4-hydroperoxycyclohexa-2,4-dien-1-one	*	S26	–	–

		6-hydroperoxycyclohexa-2,4-dien-1-one	**			-
		7-oxabicyclo[4.1.0]heptane-2,4-dione	**		–	–
		cyclohexane-1,3,5-trione	**		–	X
130	$C_6H_{10}O_3$	βKHP	?	Figure 10	–	X
		δKHP	?		–	–
		AnHP	*		–	X
		γKHP	**		–	X
		CE12HP3	?		–	X
		CE12HP4	?		–	
		4m-CEHP	?		–	–
		5m-CEHP	**		–	–
144	$C_6H_8O_4$	3-hydroperoxycyclohexane-1,5-dione	***	S27	–	x
		trans-3,6-dihydro peroxycyclohexa-1,4-diene	*		–	x
146	$C_6H_{10}O_4$	cyclohex-4-ene-1,3-diperoxol	*	Figure 15	–	x
148	$C_6H_{12}O_4$	1,3-dihydroperoxycyclohexane	*	S25	–	x
162	$C_6H_{10}O_5$	3,5-bis(hydroperoxy)cyclohexan-1-one	?	` Figure 15	–	x
		6-oxabicyclo[3.1.1]heptane-2,4-diperoxol	*			x

[a] qualitative indication: *** = very confident, ** = confident, * = likely, ? = unclear assignment

[b] conditions: JSR, τ = 2s, T = 500 – 1100 K, p = 1.07 bar, ϕ = 0.5, 1.0, 2. Only the data at low T < 630K and ϕ = 0.5, 1.0 were considered

[c] conditions: JSR, τ = 4s, T = 500 – 750 K (GC-MS) and 510 – 835 K (PIMS), p = 1.04 bar, ϕ = 0.25

[d] "X" = detected and assigned or predicted, "—" not detected or not predicted, "D" = signal detected but not assigned

The mass spectrum shown in Figure 1 contains clearly more data than what is listed in Table 1 with unpaired masses for instance. That additional information could be evaluated in a future study, e.g., to further refine the cyclohexane LTO model. In general, the species assignments agree well with those by Zou et al.[8], both their experimental assignments and those from modelling. A more detailed discussion highlighting minor differences follows hereafter. Serinyel et al.[10] did not report any species with a m/z larger than 100 and several species and/or isomers with lower m/z are missing. However, all the species identified by Serinyel et al.[10] at low temperatures (< 630 K) under lean or stoichiometric conditions are confirmed in the present study, except for cyclopenta-1,3-diene (m/z 66).

All the molecular species at m/z < 72 contain less than six carbon atoms and are therefore products from decomposition reactions. Most of them are readily and unambiguously identified and their SPES are reported as SM. The SPES measured in the present study agree particularly well with literature data for ethene (m/z = 28, Figure S5), hydrogen peroxide (m/z = 34, Figure S6), propene and ketene (m/z = 42, Figure S7), acetaldehyde and oxirane (m/z = 44, Figure S8), prop-2-enal (m/z = 56, Figure S9) and acetic acid (m/z = 60, Figure S10). Note that carbon monoxide (CO) cannot be detected at m/z 28 in this work because its ionization energy (IE=14.01 eV)[44] is outside of the scanned photon energy range.

Before discussing fuel-specific hydroperoxides, small alkyl hydroperoxides already observed by Zou et al.[8] and during the low-temperature chemistry of alkanes[45], were also detected in this work. Figures S6, S11, and S12 show the SPES of *m/z* 34, 48 and 62 respectively in agreement with reference spectra of H_2O_2 (hydrogen peroxide), CH_3-OOH (methyl hydroperoxide), and C_2H_5-OOH (ethyl hydroperoxide) from the literature. Figures S13 and S14

show also SPES of m/z 74 and 88 respectively in agreement with reference spectra of C_3H_5-OOH (allyl hydroperoxide) and C_4H_7-OOH (butenyl hydroperoxide). The detection of the latter alkyl hydroperoxides is in agreement with the work of Zou et al.[8] even if their formation were not discussed.

Species isomeric discrimination according to the most important reaction pathways

Following the pathways displayed in the flow rate analysis of Figure 3, the isomeric differentiation of species at m/z > 72 are discussed hereafter. All the flow rate analyses displayed hereafter or in SM were computed using the model of Zou et al.[8].

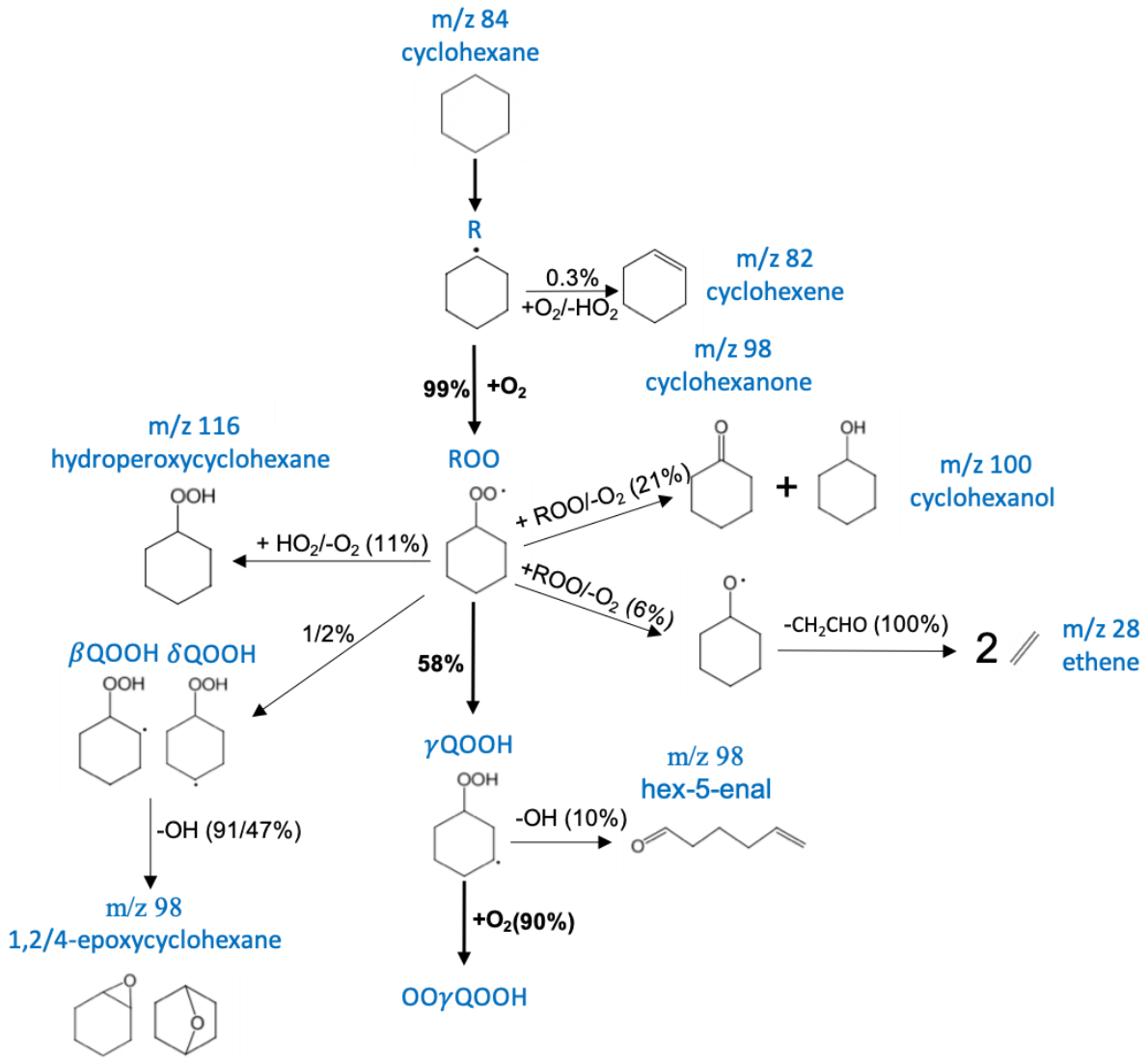

Figure 3. Flow rate analysis for cyclohexane oxidation up to the formation of OOQOOH radicals (ϕ = 0.8, 0.01 in He) at 570 K, P = 1.07 bar, and τ = 3 s. Bold arrows indicate the dominant pathways.

Chemistry deriving from cyclohexyl radicals (R)

The LTO of cyclohexane starts by the formation of cyclohexyl radical (R) that mainly further reacts with O_2 to form a cyclohexylperoxy (ROO) radical (see Figure 3. Flow rate analysis for

cyclohexane oxidation up to the formation of OOQOOH radicals (ϕ = 0.8, 0.01 in He) at 570 K, P = 1.07 bar, and τ = 3 s. Bold arrows indicate the dominant pathways.). In addition, a minor channel leads to the elimination of HO_2 and the formation of cyclohexene (C_6H_{10}, m/z 82). However, one would notice the large signal of m/z 82 in Figure 1. Comparable to the signal of m/z 85 which is 7% of m/z 84, the pathway leading to cyclohexene seems to be underestimated unless the photoionization cross section of cyclohexene is significantly higher than other species between 10 and 11 eV. Figure 4 shows the SPES of m/z 82 compared to a reference spectrum of cyclohexene from the literature[46] and simulated spectra of cyclohexene and methylidenecyclopentane. The experimental spectrum agrees with the profile from cyclohexene. The cyclohexene photoelectron spectrum by Kimura[46] is shown in Figure 4 serves as test of the simulation quality. Methylidenecyclopentane is an expected minor product from the decomposition of hex-5-enal (see Figure S15) and its simulated spectra shows that its contribution cannot be fully discarded at the present experimental conditions due to the overlap with the spectrum of cyclohexene. Our interpretation is consistent with the fact that Serinyel et al.[10] and Zou et al.[8] only reported the presence of cyclohexene at m/z 82. More discussion about products deriving from cyclohexene is given in SM.

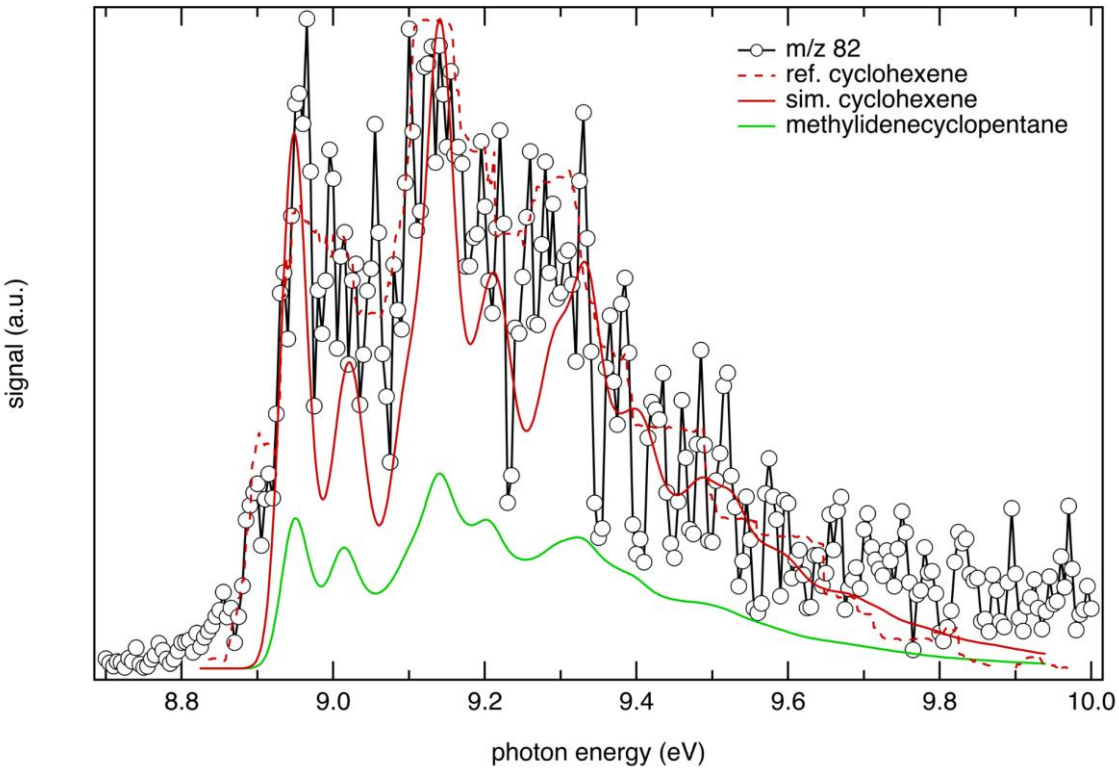

Figure 4: SPES of m/z 82 (black circles) recorded at ϕ = 0.8 and T = 570 K during the LTO of cyclohexane, compared to a reference photoelectron spectrum of cyclohexene from Kimura et al.[46] (dashed red line) and simulated spectra of cyclohexene (red line) and methylidenecyclopentane (green line). The simulated spectra have been shifted by 40 and 55 meV, respectively.

Chemistry deriving from cyclohexylperoxy (ROO) and hydroperoxycyclohexyl (QOOH) radicals

As shown in Figure 3 the predicted dominant pathway from the ROO radical is isomerization through intramolecular H-atom transfer to form a QOOH radical. However, the ROO radical is also predicted to undergo several minor pathways leading to oxidation intermediates including hydroperoxides.

Detection of hydroperoxycylohexane

As shown in Figure 3, hydroperoxycylohexane ($C_6H_{12}O_2$, m/z 116) can easily be formed via H-abstraction reactions by the ROO radical, e.g. from HO_2 radicals. A strong signal is observed at m/z 116 (see Figure 1). A possible candidate for this signal is hydroperoxycylohexane, as already proposed by Zou et al.[8] The m/z 116-selected SPES recorded during the experiments at SOLEIL is shown in Figure 5, together with a simulated spectrum of hydroperoxycylohexane. The theoretical spectrum shows a long vibrational progression due to the population of the cationic vibrational levels associated with the OO stretching mode.

The slope is consistent with that of the experimental spectrum but the calculated spectrum requires a 180 meV shift to overlap with the experimental spectrum. Such a shift is higher than the conventionally assumed uncertainty of the AIE

calculated at the CBS-QB3 level of theory. Furthermore, the AIE values at the CCSD(T)-F12 level of theory confirm the CBS-QB3 results. Recent studies in the literature showed that hydroperoxides, which exhibit significant level of flexibility, are complicated cases for computations[47]. However, as discussed hereafter triple oxygenated C_5 species have been found to exhibit similar ionization threshold as the experimental spectrum (see Figure 5).

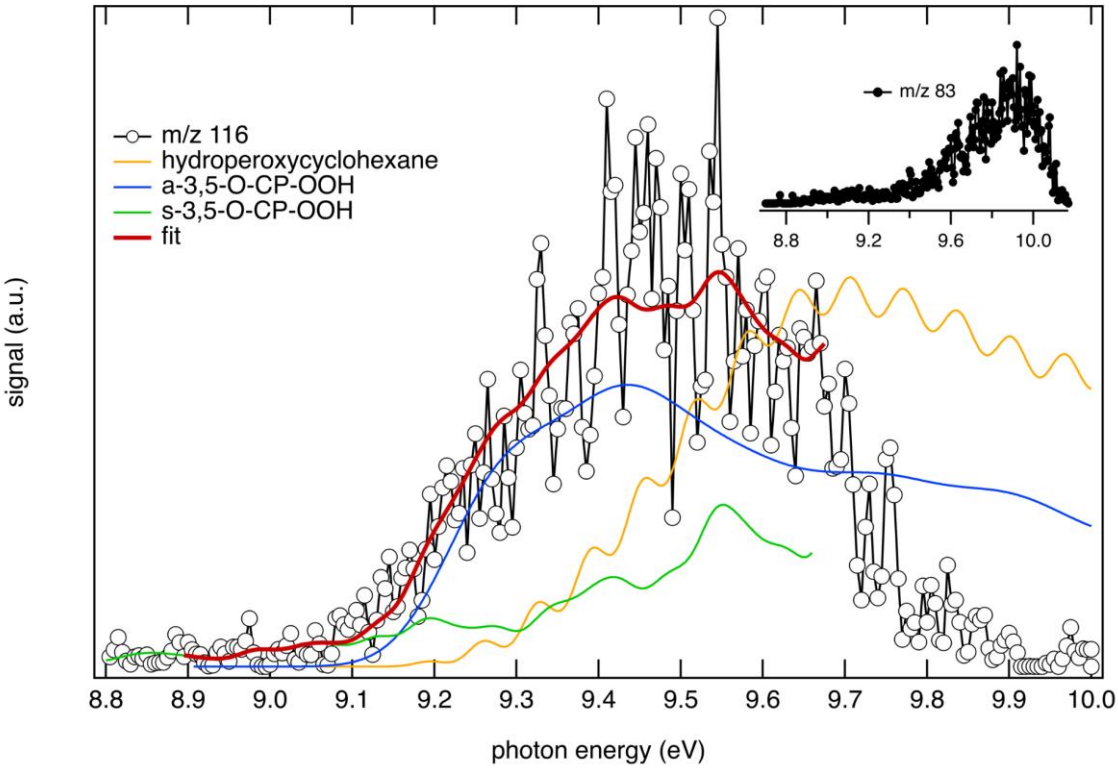

Figure 5: SPES of m/z 116 (black circles) recorded at ϕ = 0.8 and T = 570 K during the LTO of cyclohexane, compared to simulated spectra of anti- (blue line) and syn- (green line)

3,5-epoxy-cyclopentyl hydroperoxides, and hydroperoxycyclohexane (orange line). The red line is a weighed combination of the two reference spectra using a 0.6:1.0 signal ratio (cis 3,5-epoxy-cyclopentyl hydroperoxides:trans 3,5-epoxy-cyclopentyl hydroperoxides). The computed syn-isomer spectrum has been shifted by 50 meV. The inset shows the SPES of m/z 83 (black dots).

Recently, Sheps et al.[48] studied the LTO of cyclopentane and they provided AIEs for numerous second oxygen addition products. Among those, the calculated AIEs and PES of cis- and anti-3,5-epoxy-cyclopentyl hydroperoxide (3,5-O-CP-OOH, m/z 116) agree well with the present experimental SPES (see Figure 5). Note that the calculated AIEs reported in this work at the CBS-QB3 level of 9.07 and 8.71 eV for the anti- and cis-isomers, respectively, agree well with the higher level calculations reported by Sheps et al.[48]. This indicates that the CBS-QB3 method is generally sufficiently accurate for this type of calculations. The kinetic model of Zou et al.[8] does not predict these hydroperoxides but their contributions cannot be excluded and potential formation pathways are discussed at the end of the results section.

For photon energies ≥ 9.7 eV, the measured m/z 116 signal falls below the simulated spectra of hydroperoxycyclohexane and the three times oxygenated C5 species. Given that hydroperoxides tend to fragment easily upon photoionization[12,14], the discrepancy between the experimental and calculated spectra at higher energies is plausible, because the calculations do not account for fragmentation. This explanation is consistent with the observed broadening of the m/z 83 signal (see Figure 1: Typical time-of-flight mass spectrum obtained by integration over the photon energy range from 10.0 to 11.0 eV with a step size of 5 meV and an acquisition time of 80 s per step during the LTO of cyclohexane at ϕ = 0.5 and T = 590 K), the peak width being proportional to the square root of the cation's translational energy and thus indicative of a fragmentation event. In fact, the m/z 83 signal increases when m/z 116 peak intensity is maximum and reaches its maximum when m/z 116 peak vanishes. This fragment cation is formed from the parent cation upon HO_2 release.

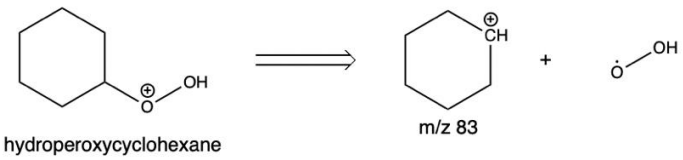

Figure 6. Suggested dissociative ionization pathway of hydroperoxycyclohexane.

Discrimination between mono-oxygenated cyclohexane isomers

As shown in Figure 3, the different QOOH radicals produce different cyclic ethers after the release of an OH radical. βQOOH and δQOOH produce 1,2-epoxycyclohexane and 1,4-epoxycyclohexane, respectively. The electronic footprints of both species were detected in the SPES of m/z 98 (see Figure 7). γQOOH is the most likely formed radical due to the low energy barrier for its formation[9].It is mainly consumed via reaction with a second oxygen molecule. Unimolecular decomposition of γQOOH is a minor channel, which produces hex-5-enal and an OH radical. The detection of hex-5-enal cannot be fully confirmed by the SPES of m/z 98 due to the number of isomers and the low signal to noise ratio (see Figure 7). The calculated AIEs of 1,2-epoxycyclohexane and hex-5-enal are very similar which leads to an overlap of their simulated spectra over most of the energy range, but the simulation of the

SPES of m/z 98 yields a higher weight on 1,2-epoxycyclohexane. More discussion about products possibly deriving from 1,2-epoxycyclohexane is given in SM.

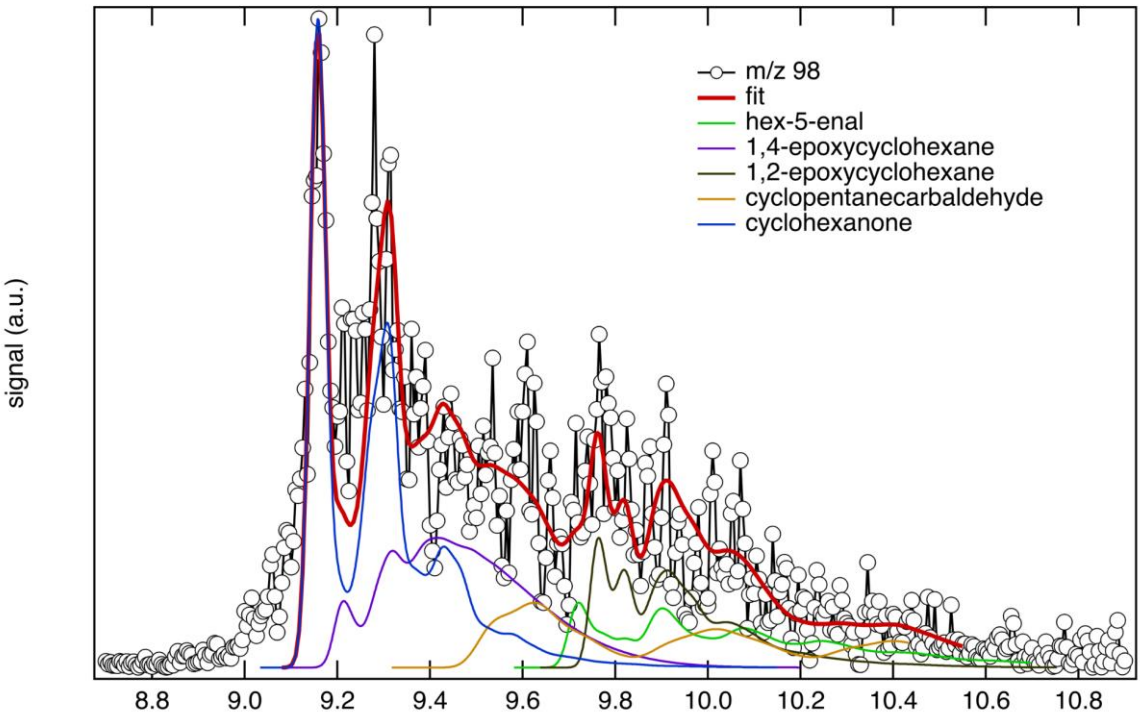

Figure 7: Experimental SPES of m/z 98 (black circles) recorded at ϕ = 0.8 and T = 570 K during the LTO of cyclohexane, compared to simulated spectra of cyclohexanone (blue line), 1,4-epoxycyclohexane (purple line), cyclopentanecarbaldehyde (orange line), hex-5-enal (green line), and 1,2-epoxycyclohexane (brown line). The red line is a weighed combination of the simulated spectra using 1.0:0.2:0.2:0.1:0.1 signal ratio (cyclohexanone:1,4-epoxycyclohexane:1,2-epoxycyclohexane:cyclopentanecarbaldehyde:hex-5-enal). The simulated spectra of cyclohexanone, cyclopentanecarbaldehyde, hex-5-enal, and 1,2-epoxycyclohexane have been shifted by 50, 60, 13, and 30 meV, respectively.

Another predicted important ROO reaction channel is the bimolecular reaction of peroxy radicals (see Figure 3). ROO + ROO reactions are predicted to be mainly produce cyclohexanone ($C_6H_{10}O$, m/z 98), cyclohexanol ($C_6H_{12}O$, m/z 100) and O_2. Concerning m/z 98, Figure 7 shows the SPES for m/z 98 together with several experimental or simulated spectra for $C_6H_{10}O$ isomers which include C_6-ring molecules, hex-5-enal, which is formed via ring opening of the γQOOH, and cyclopentanecarbaldehyde. All five isomers considered have been detected by Serinyel et al., whereas Zou et al.[8] have identified all species except cyclopentanecarbaldehyde. A least-squares fit of the simulated spectra to the SPES of m/z 98 shows that the SPES of m/z 98 contains mostly the cyclohexanone signature. The reference PES of cyclohexanone from Tian et al.[49] is in good agreement with the theoretical calculations performed in this work. The other detected isomers should be taken with caution du to the low signal to noise ratio.

Concerning m/z 100, a signal is clearly detected in the current study and by Zou et al.[8], who did not assign it. Serinyel et al.[10] identified cyclohexanol as a product in their GC study. Figure 8 shows the measured SPES spectrum together with simulated spectra for cyclohexanol

and the $C_5H_8O_2$ isomers 3-hydroperoxycyclopentene and 4-hydroperoxycyclopentene. An attempt to reproduce the experiment solely with the simulated cyclohexanol spectrum would require an energy shift above 200 meV, which exceeds of the expected uncertainty of our theoretical simulation. The inclusion of other cyclohexanol conformers, taken from Tian et al.[49], does not lead to improvements. In contrast, the SPES of m/z 100 is well reproduced if one considers the presence of 3-hydroperoxycyclopentene and 4-hydroperoxycyclopentene and includes their simulated spectra in the fitting procedure. Optimal agreement between measured and simulated spectra shows cyclohexanol contributing the least and 4-hydroperoxycyclopentene the most to the spectrum. Indeed, the signal ratio is too low to allow for an unambiguous identification of cyclohexanol. The kinetic model of Zou et al.[8] does not predict these C5-hydroperoxides, but one can explain their formation from the secondary chemistry of hex-5-enal (see discussion in SM).

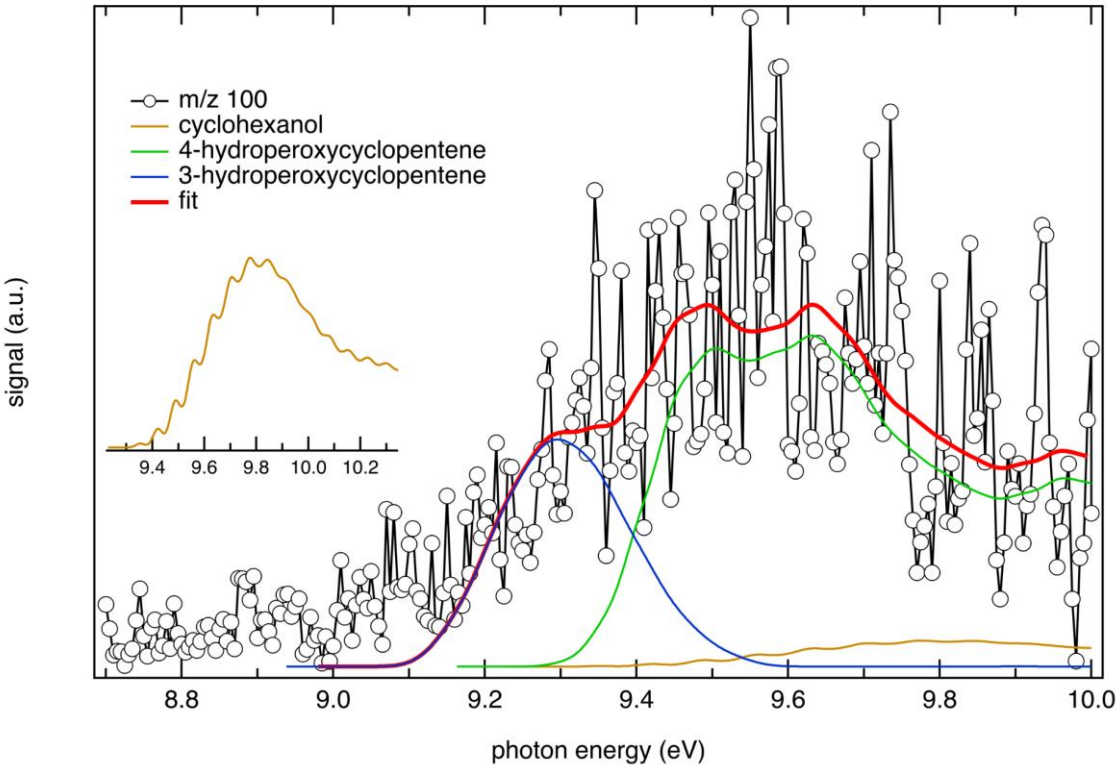

Figure 8: Experimental SPES of m/z 100 (black circles) recorded at ϕ = 0.8 and T = 570 K during the LTO of cyclohexane, compared to simulated spectra of cyclohexanol (orange line), 3-hydroperoxycyclopentene (blue line), and 4-hydroperoxycyclopentene (green line). The red line is a weighed combination of the simulated spectra using 0.1:0.7:1.0 signal ratio (cyclohexanol:3-hydroperoxycyclopentene:4-hydroperoxycyclopentene). The inset shows a blown-up view of the simulated spectrum of cyclohexanol.

As shown in Figure 3, a second minor ROO + ROO reaction pathway leads to the formation of two cycloalkoxy radicals (RO) and O_2. According to the Zou model, RO decomposes yielding two ethene (m/z 28) molecules and a vinoxy (CH_2CHO) radical. The vinoxy radial is a source of ketene (m/z 42). As previously discussed, ethene and ketene are well identified products in this work.

Chemistry deriving from the addition of O_2 to QOOH

The QOOH radicals play a crucial role in the autoignition process as they can undergo a second addition to oxygen producing hydroperoxycyclohexylperoxy radical (OOQOOH). As shown in Figure 9, the kinetic model of Zou et al.[8] predicts that the OOQOOH decomposition pathways are different regarding the respective cis-/trans- conformation.

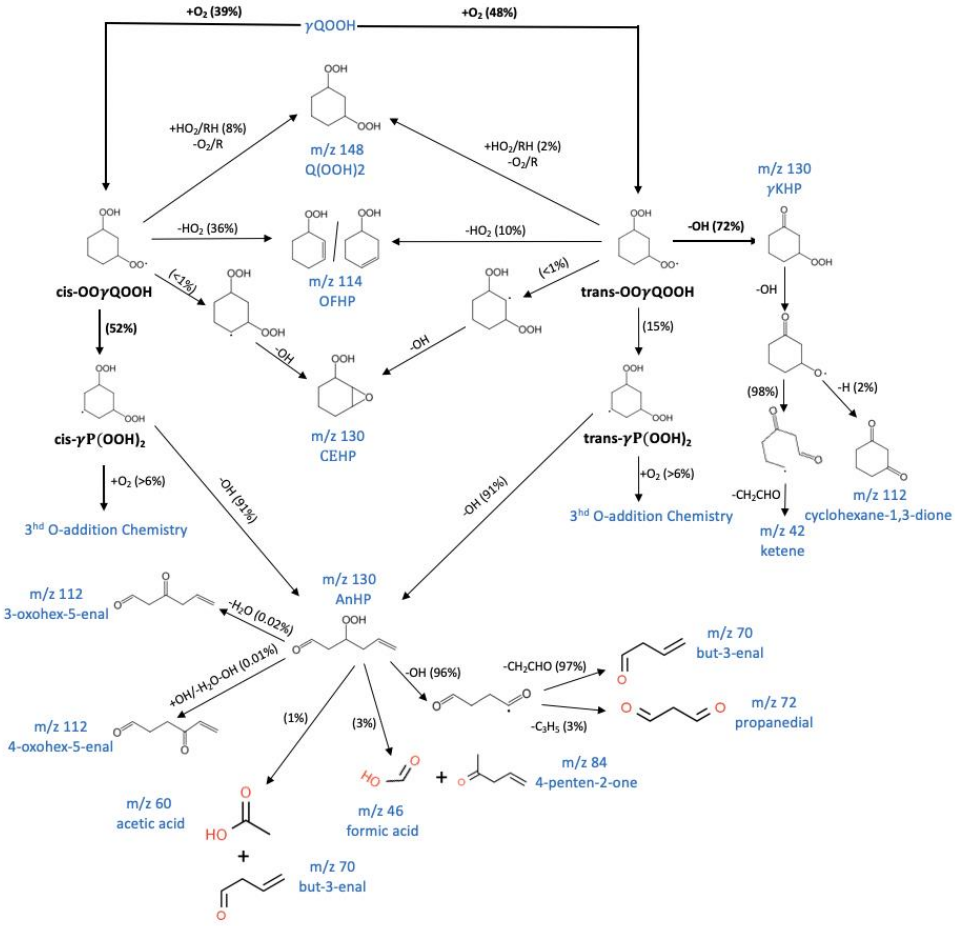

Figure 9. Flow rate analysis of the consumption of γQOOH chemistry by O_2 addition up to the 3rd O_2-addition during cyclohexane oxidation (ϕ= 0.8, 0.01 in He) at 570 K, P = 1.07 bar, and τ = 3 s). Bold arrows indicate the predicted dominant pathways at these conditions.

Detection of ketohydroperoxides

According to Figure 9, the kinetic model predicts that the trans-OOγQOOH mainly decomposes into a γKHP, 3-hydroperoxycyclohexan-1-one ($C_6H_{10}O_3$, m/z 130) by releasing an OH radical. Of significant importance is the relatively large signal at m/z 130 because it is potentially composed of several isomers: cyclic KHPs, hydroperoxycyclic ether (CEHP) and acyclic unsaturated KHPs or unsaturated hydroperoxyaldehydes (AnHP). The relative composition of these species reflects the competition between ring-opening (β-scission) reactions and intramolecular H-abstraction reactions (followed by cyclic ether or keto group formation) of the $P(OOH)_2$ intermediate (cf. Figure 9).

Most of the $C_6H_{10}O_3$ isomers considered in this work have calculated AIEs starting around 9.2 eV or above (see Table S1) but the ionization threshold observed on the SPES of m/z 130 starts around 9 eV (see Figure 10). Zou et al.[9] consider γKHP to be the most likely

isomer. Adiabatic Ionization energy (AIE) calculations by Zou and in this current work for γKHP conformers yielded AIEs from 9.2 to 9.4 eV.

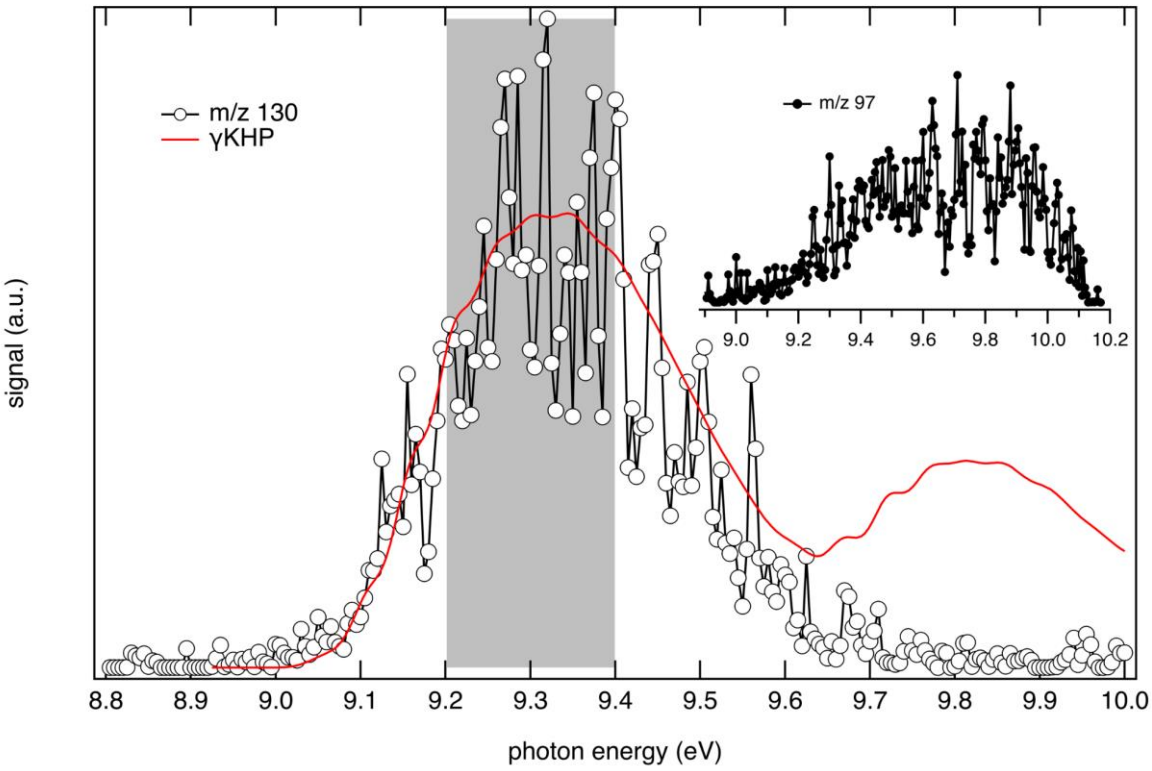

Figure 10: Experimental SPES of m/z 130 (open circles) recorded at ϕ = 0.8 and T = 570 K during the LTO of cyclohexane and compared to simulated spectra of γKHP. The shaded box indicates the spread in the (unshifted) calculated AIE of γKHP conformers. The inset shows the SPES of m/z 97 (black dots). The simulated spectrum of γ-KHP has been shifted by 135 meV.

Upon photoionization of γ-KHP, the corresponding cation may potentially eject a HO_2 fragment to form a m/z 97 cation (as discussed above for m/z 116):

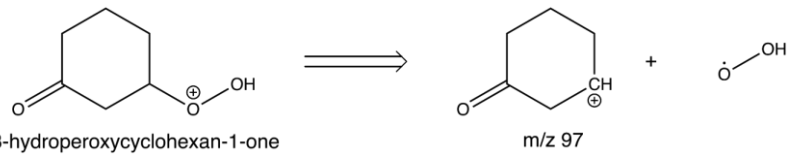

Figure 11. Suggested dissociative ionization pathways of γ-KHP.

The peak at m/z 97 is substantially broader than those for m/z 96 and m/z 98, which is characteristic of a fragment peak (see Figure 1: Typical time-of-flight mass spectrum obtained by integration over the photon energy range from 10.0 to 11.0 eV with a step size of 5 meV and an acquisition time of 80 s per step during the LTO of cyclohexane at ϕ = 0.5 and T = 590 K. The vertical scale is reduced to zoom out the low intensity peaks so that cyclohexane (m/z 84) and its 7% ^{13C} isotopomer (m/z 85) are cut off.). Accordingly, the simulated spectrum of γKHP shown in Figure 10 should be compared to the sum of the experimental spectra of m/z 130 and m/z 97. Assuming a 135 meV energy shift, the first part of the simulated spectrum of

γKHP, below 9.6 eV, fits the SPES of m/z 130 while the second part, above 9.6 eV, nicely fits with the SPES of m/z 97 with a maximum around 9.8 eV. The coherence of the signal of both masses supports the identification of γKHP as the main contributor in the SPES signature in the m/Z 130 mass channel.

Given the complexity of the reaction pathways shown in Figure 9, additional interpretation of the m/z 130 signal requires comparison with other simulated spectra of the many other possible products. This will be anything but straightforward. Among the 10 $C_6H_{10}O_3$ isomers listed in Table S1 with their structures, symbolic names and AIEs, all the expected products have an AIE that is similar or higher than the observed ionization energy threshold. Consequently, none of these species can be easily excluded. The experimental ionization threshold fits with the AIE of trans- and cis-5m-CEHP, suggesting the CEHP of the tetrahydrofuran type can be produced but the formation of these species in notable amount is unlikely according to the theoretical kinetic calculations of Zou et al.[9]. Interestingly, Zou et al.[8] assigned their m/z 130 signal to ketohydroperoxides (KHP), acyclic unsaturated hydroperoxyaldehydes (AnHP) and oxirane-type CEHP. Our results are consistent with the dominant formation of γKHP, although other $C_6H_{10}O_3$ isomers may certainly be present as well.

Detection of the products obtained by KHP degradation

As shown in Figure 9, γKHP has two decomposition channels. O-O bond scission yields a ketoxy radical, which mainly decomposes by C-C β-scission to produce ethene and two ketene (C_2H_2O, m/z 42) molecules. Figure S7 shows the SPES of m/z 42, with a fit using reference literature spectra of ketene (C_2H_2O) and propene (C_3H_6). The literature spectra of both molecules were summed and weighted with appropriate factors to fit the measured SPES in the appropriate photon energy range. Relative mole fractions could then be estimated by weighting the branching ratio using the absolute photoionization cross sections at 10.0 eV from Yang et al.[50] for ketene (22.4 Mb) and Person et al.[51] for propene (7.2 Mb). The weighting leads to a ketene:propene relative mole fraction ratio of 0.8:1.0 suggesting that ketene is present in similar amount than propene. This result is in good agreement with the 1.0:1.0 mole fraction ratio of ketene:propene predicted by the kinetic model of Zou et al.[8]

A minor channel from γKHP via C-H β-scission leads to cyclohexane-1,3-dione ($C_6H_8O_2$, m/z 112). The SPES spectrum obtained for m/z 112 together with predicted spectra for several $C_6H_8O_2$ species is shown in Figure 12. For these calculations, we considered the molecular species playing a role in the kinetic model by Zou et al.[8], namely cyclohexane-1,3-dione, cyclohexane-1,2-dione, 4-oxohex-5-enal, 3-oxohex-5-enal, and cyclohexane-1,4-dione. All these species may be formed via decomposition of KHPs and other $C_6H_{10}O_3$ (linear) isomers. The high contribution of 1,3-cyclohexanedione supports the formation of γKHP during the LTO of cyclohexane. Zou et al.[8] assigned their m/z 112 signal to 1,3-cyclohexanedione and 3-oxohex-5-enal, which agrees with our analysis which also includes the likely presence of 4-oxohex-5-enal.

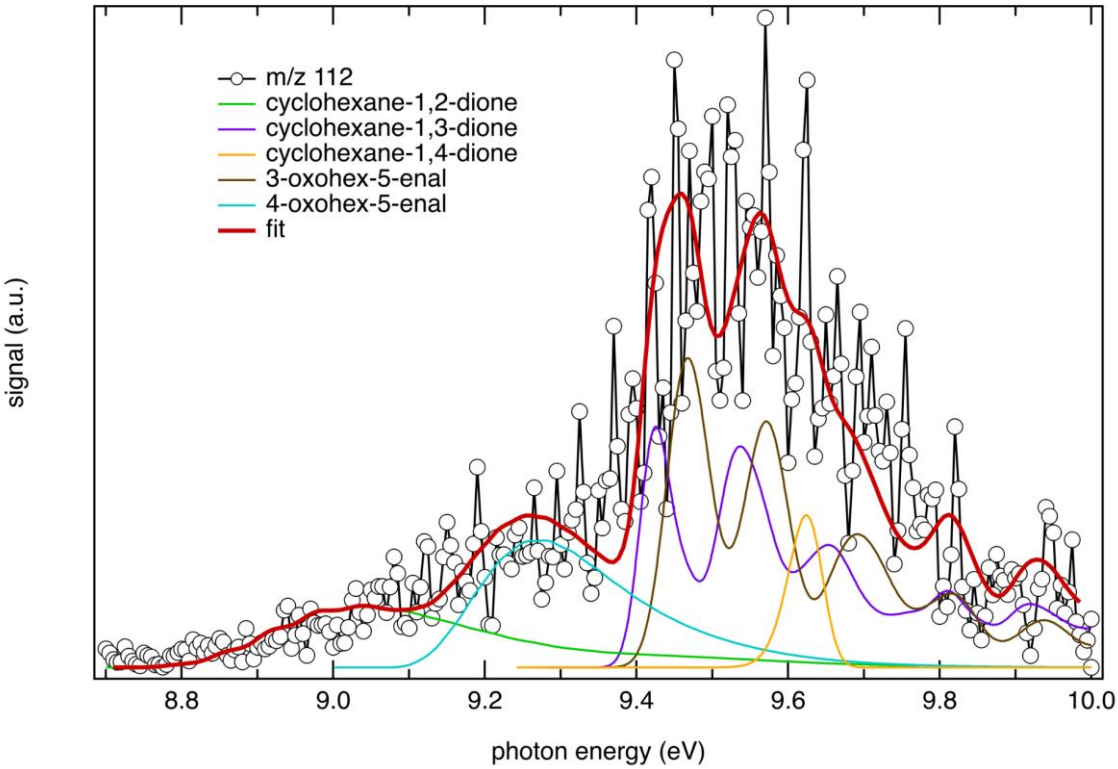

Figure 12: Experimental SPES of m/z 112 (black circles) recorded at ϕ = 0.8 and T = 570 K during the LTO of cyclohexane compared to simulated spectra. The red line is a weighted combination of the simulated spectra using 0.2:0.4:0.8:1.0:0.4 signal ratio (1,2-cyclohexanedione:4-oxohex-5-enal:1,3-cyclohexanedione:3-oxohex-5-enal: 1,4-cyclohexanedione). The simulated spectrum of 3-oxohex-5-enal was shifted by 30 meV.

AnHP is certainly another important m/z 130 isomer even if its formation could not be fully proven by the SPES analysis. According to Figure 9, the alkoxy radical deriving from AnHP mostly undergoes β-scission and forms but-3-enal (C_4H_6O, m/z 70), a species detected in this work, see Figure S22. Another minor decomposition product of the alkoxy radical deriving from AnHP is propanedial ($C_3H_4O_2$, m/z 72). Figure S23 shows the SPES of m/z 72 compared to reference spectrum of propanedial and confirms the formation of this species, even if that of other C_4H_8O isomers, tetrahydrofuran (oxolane), butanal, and 2,2-dimethyloxirane, cannot be fully discarded. Note that these three C_4H_8O isomers are not predicted by the kinetic model for our experimental conditions, but they were detected in the experimental work of Zou et al.[8].

Figure 9 also shows the occurrence of the Korcek mechanism, which is a KHP decomposition pathway via an intermediate cyclic peroxide leading to the formation of a carbonyl compound and an organic acid[52]. A first channel involves the formation of but-3-enal (C_4H_6O, m/z 70) and acetic acid ($C_2H_4O_2$, m/z 60) as co-product. Both species were detected in this work as can be seen Figure S10 and Figure S22 for acetic acid and but-3-enal, respectively. A second channel yields pent-4-en-2-one (C_5H_8O, m/z 84) and formic acid (CH_2O_2, m/z 46). Figure S24 shows the SPES of m/z 46 recorded in this work acquired during a relatively quick mass spectrum acquisition of 30 min at a fixed photon energy of 11.5 eV. Despite the low signal-to-noise ratio, an unambiguous ionization threshold is observed, fitting with the first peak of formic acid. In Figure S4, the SPES of m/z 84 corresponds mainly to cyclohexane but a small signal increase is visible at a photon energy slightly above 9.2 eV, which is clearly below

the ionization threshold for cyclohexane (9.87 eV[41]). Zou et al.[8] interpreted the m/z 84 signal in their comparable, but leaner (ϕ=0.25), cyclohexane LTO study with contributions from pent-4-en-2-one. The simulated PES supports this interpretation but the low signal-to-noise prevents an unambiguous identification of such compound.

As shown in Figure 9, two products at m/z 112 are formed via very minor channels from AnHP, namely 3-oxohex-5-enal and 4-oxohex-5-enal. The 3-oxohex-5-enal:4-oxohex-5-enal signal branching ratio deduced in this work is in good agreement with the predicted branching ratio from the kinetic model of Zou et al.[8] if one assumes similar photoionization cross sections.

Detection of other QOOH + O_2 products

Figure 9 shows an additional OOγQOOH reaction pathway with the release of a HO_2 group leading to 3-hydroperoxycyclohexene and 4-hydroperoxycyclohexene. Those species have been detected in the SPES of m/z 114 as shown in Figure 13. Also, this figure shows the SPES of m/z 114 recorded during the SOLEIL experiments compared to simulated photoelectron spectrum of hexanedial and two olefinic hydroperoxides (OFHP), which are 3-Hydroperoxycyclohexene and 4-hydroperoxycyclohexene. The latter are expected oxidation products mainly from hydroperoxycyclohexyl radical (QOOH) chemistry. From Figure 13 it is clear that 4-hydroperoxycyclohexene is the major contributor to the SPES of m/z 114, but 3-hydroperoxycyclohexene is necessary to reproduce at least the experimental signal around 9.2 eV, while the formation of hexanedial is less obvious. According to the analysis by Zou et al.[8], all three isomers are present. Nevertheless, the poor agreement between simulated and measured SPES in the 9.0 – 9.2 eV region might indicate that at least one additional m/z 114 species contributes to the spectrum.

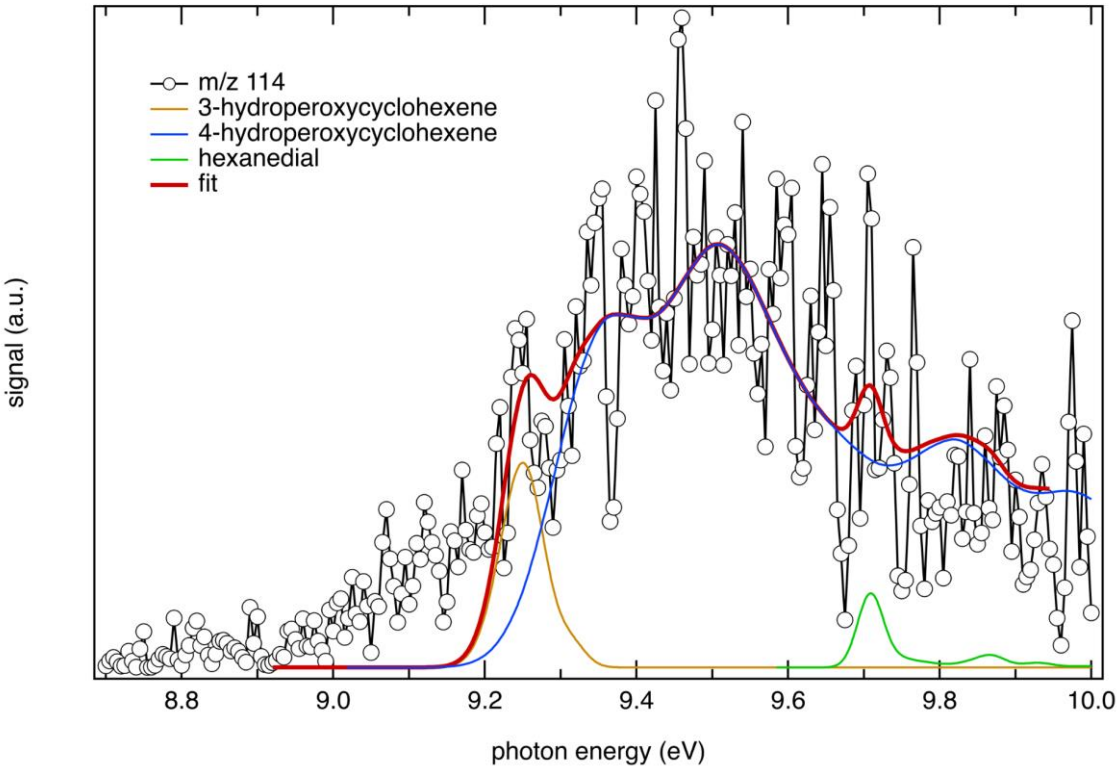

Figure 13: Experimental SPES of m/z 114 (black circles) recorded at ϕ = 0.8 and T = 570 K during the LTO of cyclohexane, compared to simulated spectra. The red line is a weighed combination of the three reference spectra using 0.5:1.0:0.2 signal ratio (3-hydroperoxycyclohexene:4-hydroperoxycyclohexene:hexanedial). The simulated spectra have been shifted by 80, 70, and 13 meV, respectively.

The kinetic model also suggests the occurrence of bimolecular reactions between OOγQOOH and HO_2/RH leading to 1,3-dihydroperoxycyclohexane ($C_6H_{12}O_4$, m/z 148). A VMI-PES of m/z 148 recorded in this work is shown in Figure S25. The PES of m/z 148 has a low resolution because it was recorded at a fixed photon energy of 10.0 eV during a 90 minutes acquisition of a mass spectrum in order to improve the signal-to-noise ratio for heavy species, above m/z 130 (see Figure S3). The calculated AIE of the conformer with both OOH groups in the axial position fits with the ionization threshold of the experimental spectrum but the low resolution prevents further analysis (see Table S2). Note that those reactions are incorporated into the kinetic model of Zou et al.[8] with rate constants referred to similar reactions in the first oxygen addition stage and should, perhaps, be revised.

Chemistry induced by the third O_2-addition

According to the finding of Wang et al. during the LTO of alkanes[43,53] and cycloalkanes[54], the $\gamma P(OOH)_2$ radical obtained by isomerization of the OOγQOOH may undergo a third oxygen addition and contributes to chain branching (see Figure 14). Similar to the second oxygen addition, the third oxygen addition to $\gamma P(OOH)_2$ may occur at axial or equatorial position, forming cis-OO$\gamma P(OOH)_2$ or trans-OO$\gamma P(OOH)_2$ isomer.

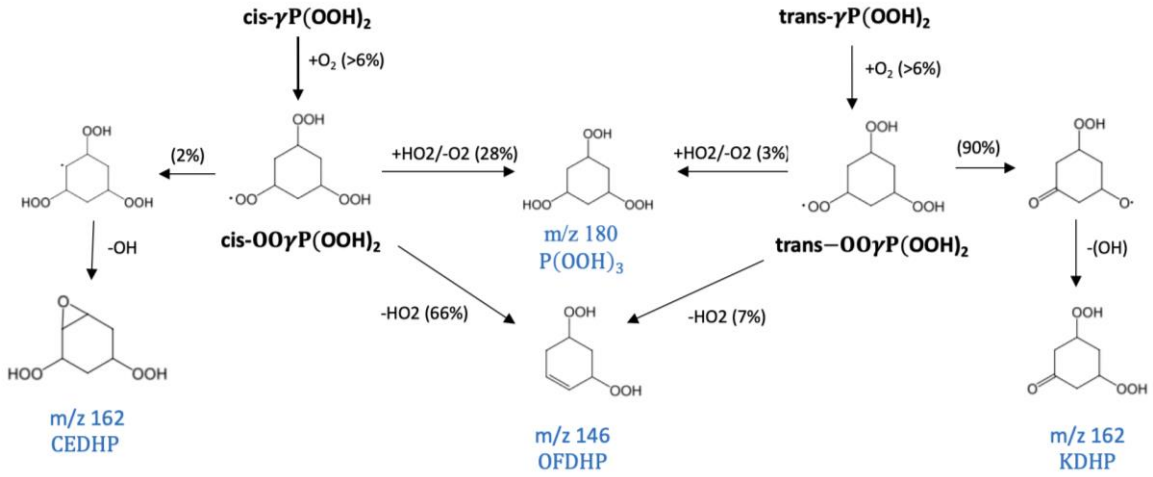

Figure 14. $\gamma P(OOH)_2$ chemistry after the third O_2-addition.

The trans-OO$\gamma P(OOH)_2$ isomer is predicted to mainly undergo conventional isomerization to form ketodihydroperoxide (KDHP, m/z 162) and ultimately results in chain branching. A weak signal was detected at m/z 162, which is shown in Figure 15 (left) together with the AIE of a cyclic ether dihydroperoxide isomer (labeled as CEDHP) that carries one OOH group on axial position and one OOH group on equatorial position. However, the calculated AIEs of KDHP isomers were found to be higher than the experimental ionization threshold (see

Table S3). Besides, the assignment of m/z 162 to a CEDHP is in agreement with the analysis provided by Zou et al.[8] and also with predictions by their kinetic model, although the formation of KDHP is suggested to be favored. Unfortunately, the low resolution prevents further analysis except the fact that isomers other than KDHP (such as CEDHP) need to be included to explain the PES of m/z 162. We clearly reach, in this high mass range, the current limit of our PEPICO approach benchmarked with high-level calculations.

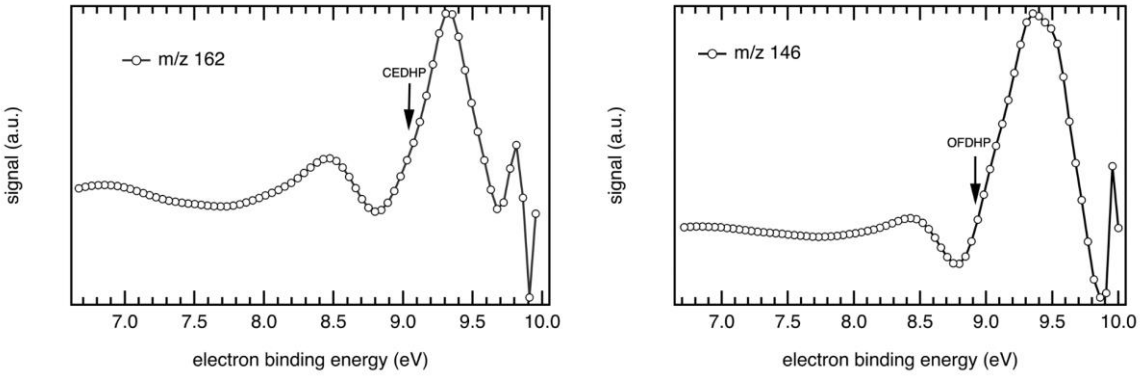

Figure 15: VMI-PES recorded at 10 eV of (left) m/z 162 (black circles) compared to the calculated AIE of a CEDHP isomer, (right) of m/z 146 (black circles) compared to the AIE of a OFDHP isomer.

On the other hand, cis-OOγP(OOH)$_2$ conformer is predicted to undergo concerted elimination to yield mainly olefinic dihydroperoxide (OFDHP, m/z 146). Even though a weak signal at m/z 146 was detected, the VMI-PES of m/z 146 agrees reasonably well with the AIE of the OFDHP that carries one OOH group on axial position and one OOH group on equatorial position (see Figure 15 (right) and Table S4). In addition, minor predicted channels from both cis- and trans-OOγP(OOH)$_2$ through bimolecular reactions with HO_2 might lead to the formation of P(OOH)$_3$ at m/z 180 but no signal for this m/z has been observed.

In this work, signals were also recorded in the m/z 126 and 144 channels, whose TIY analysis (Figure S26 and S27 respectively) highlights the presence of ketone, dione, trione, and dienone species. Signals at m/z 126 and 144 were also detected in the work of Zou et al.[8], but the low resolution did not allow conclusions on the structure of the species. Kinetic pathways should be proposed in the future to simulate the formation of these compounds in cyclohexane LTO that are missing in the current kinetic model.

Kinetic pathways for potential five-membered ring species

Overall the results of the SPES analysis are in good agreement with the predictions of the kinetic model of Zou et al.[8] even with regards to minor reaction pathways. Beyond the uncertainties which can result from a PEPICO analysis in particular in the case of signals with a low signal-to-noise ratio or for masses with many contributing isomers, this study raises the question of the formation of C_5-ring compounds during cyclohexane LTO. In the PES analysis presented here, the formation of cyclopentanecarbaldehyde (m/z 98), 3-hydroperoxycyclopentene and 4-hydroperoxycyclopentene (m/z 100), and 3,5-epoxy-cyclopentyl hydroperoxide (m/z 116) was not fully confirmed, but was neither fully ruled out. Such molecules are not predicted by the kinetic model and are not detected in previous experimental studies, apart from cyclopentanecarbaldehyde by chromatography-mass spectrometry (GC-MS)[10]. In this context, the signal at m/z 66 is also interesting, because

Serinyel et al.[10] detected cyclopenta-1,3-diene (identification by GC-MS) as a product in their lean (ϕ=0.5) and stoichiometric experiments above 605 K. Figure 1 shows no signal at m/z 66 and Figure 4 in Ref.[8] contains only a weak signal at m/z 66 that was not further analyzed. However, since all three studies report a non-zero signal at m/z 68, which could be due to cyclopentene (Serinyel et al.[10]), the presence of small amounts of cyclopenta-1,3-diene would not be surprising.

Another feature of the oxidation of cyclic species is the possibility of ring-opening reactions to compete with regular LTO pathways. Knepp et al.[55] pointed out that the ring-opening product of cyclohexyl radical, 5-hexen-1-yl, is clearly higher in energy than cyclohexyl. However, 5-hexen-1-yl may further react to form cyclopentylmethyl radicals, which is of similar stability as cyclohexyl. Hence the oxidation of cyclopentylmethyl radical may have an impact on cyclohexane LTO. Nevertheless, it seems that the most recent studies of cyclohexane LTO have not considered this possibility. **Figure 16 shows schematically the possible role that 5-membered ring alkyl radicals could play and that the conversion is feasible. Figure 16 provides the absolute energies and shows that the first barrier is with about 30 kcal/mol sufficiently low that the isomerization step is energetically possible. Furthermore, β-scission reactions have reasonably high A-factors. Detailed Master equation analysis is needed to assign rate expressions and the isomerization competes with O_2 addition, hence the O_2 concentration also determines whether isomerization may contribute.** The model of Zou et al.[8] reproduces their JSR data relatively well but O_2 addition reactions onto minor isomers of cyclohexyl radicals are not considered.

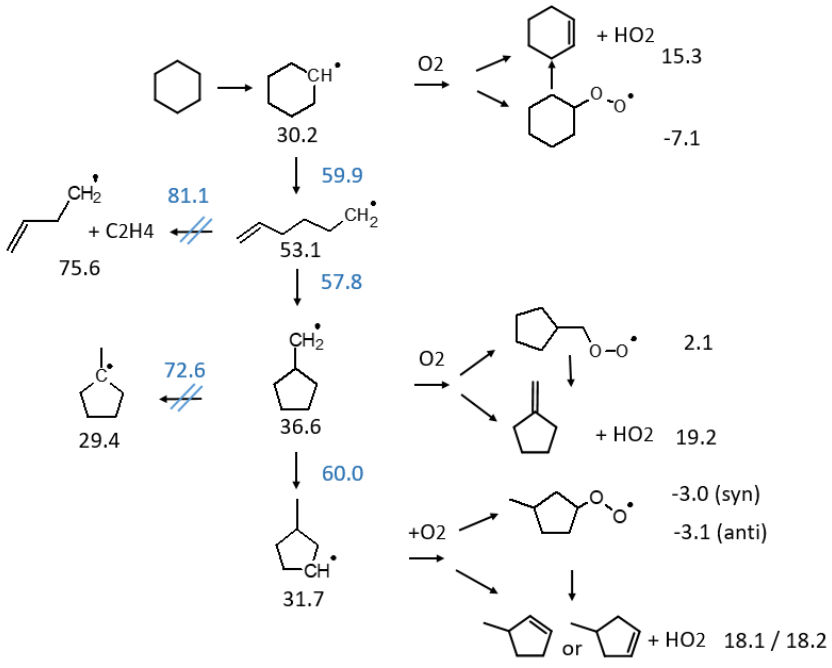

Figure 16: Possibly available initial radicals and first O_2 addition products in the LTO of cyclohexane. Heat of formation (black) and transition state enthalpies (blue) in kcal/mol calculated at the CBS-QB3 level of theory and at 570K. Note that the cycloalkenes can either be formed directly from the chemically activated adduct or after thermalization of the peroxy radical.

Methylidenecyclopentane is an expected product from the decomposition of hex-5-enal but if the cyclohexyl radical isomerizes before reacting with O_2, other C_6H_{10} isomers may be formed (see Figure 16). If C_6H_{11} isomers other than cyclohexyl play a role in cyclohexane LTO, then two additional molecules could contribute to the m/z 82 signal. These are 3-methylcyclopentene and 4-methylcyclopentene but all ionization thresholds are around 9.0 eV and the overall shapes of all four PES are quite similar. Besides, we would like to emphasize that Serinyel et al.[10] and Zou et al.[8] both showed the presence of cyclohexene, which is easily detectable by GC. These authors do not report on other C_6H_{10} isomers. However, cyclopentylmethyl radicals can isomerize after the O_2 addition to hydroperoxycyclopentylmethyl radicals which, upon removal of a methyl group, can produce hydroperoxycyclopentene isomers:

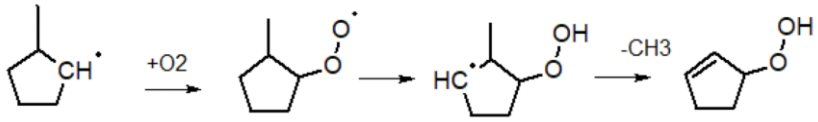

The presence of 3,5-epoxy-cyclopentyl hydroperoxide is then plausible given that hydroperoxycyclopentenes were potentially identified as a source for the m/z 100 signal. For example, HO_2 addition to 4-hydroperoxycyclopentene followed by cyclization to the oxetane would lead to m/z 116.

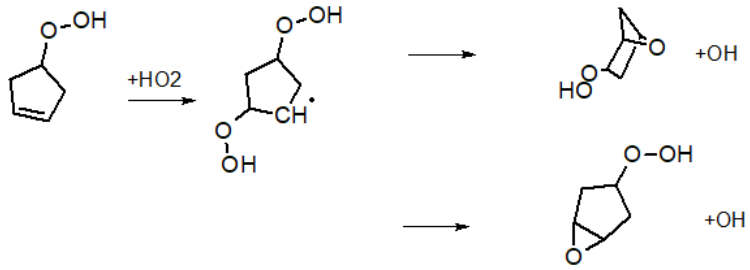

Those reactions are not included in the kinetic model of Zou et al.[8] but need to be investigated through rate constant calculations and potential energy surfaces analysis in future work to see if the formation of 5-membered ring products is important in cyclohexane LTO.

Conclusion and perspectives

Cyclohexane LTO was investigated using a JSR within the temperature range of T = 560 – 620 K and equivalence ratios between ϕ = 0.5 – 1.0. Products from the LTO of a lean cyclohexane/oxygen mixture were detected and identified with a SVUV-PEPICO analysis and high-level theoretical quantum calculations for the first time. The recording of electronic fingerprints of the products and intermediates provided experimental data with a high resolution for isomeric discrimination. The results were compared to the predictions of the newly validated kinetic model by Zou et al.[8] and the most recent experimental works on cyclohexane LTO.

Overall the present results are in good agreement with the predictions of the kinetic model of Zou et al.[8] even with regards to minor reaction pathways. Most of the predicted products and intermediates were detected, including those predicted from side reactions. The results confirm that reactive hydroperoxide channels dominate the chain-branching process under the present conditions. The main KHP (m/z 130) was detected addressing the conformational effects developed by Zou et al.[8] in cyclohexane LTO. When direct detection was not possible due to PEPICO analysis limitation (too low signal-to-noise ratio and/or masses

with too many isomers), the detection of respective decomposition products supported their identification. This allowed a more confident identification of the products from the rich chemistry of O_2-addition on QOOH radicals for which products from the third oxygen addition channels were also identified.

Our work indicates that five-membered ring species may potentially be relevant. This raises the question about missing reaction pathways in cyclohexane LTO. A comparison of the isomer information obtained from the SVUV-PEPICO experiments with expected products provided hints that substituted cyclopentyl radicals might play a minor role in cyclohexane LTO. Nevertheless, additional work needs to be done to address this question, especially PEPICO experiments at conditions optimized for species identification for m/z which could not yet be identified with confidence. Given that the Zou model works well, it would be interesting to use it predict the formation of crucial intermediates as a function of temperature and composition and to use these results as start for a new campaign to verify the predicted temperature profiles. A study focusing on the potential role of C_6H_{11} isomers other than cyclohexyl would also be helpful in light of the observations of this current study. Furthermore, SPES spectra starting at lower PI energy are needed to identify some of the easy to ionize species discussed in this work, e.g. fulvene. Such data would provide even more stringent tests for the kinetic model and help to identify potential gaps in our understanding of the cyclohexane LTO.

Acknowledgements

We are grateful to the whole SOLEIL staff for smoothly running the facility under project 20201093. The authors thank the QUADMARTS International Research Network for promoting their collaboration. HHC acknowledges I3A for the use of its HPC cluster HERMES and the funding from the Aragón Government (Ref. T22_20R), co-funded by FEDER 2014-2020 "Construyendo Europa desde Aragón".

References

(1) Zádor, J.; Taatjes, C. A.; Fernandes, R. X. Kinetics of Elementary Reactions in Low-Temperature Autoignition Chemistry. *Progress in Energy and Combustion Science* **2011**, *37* (4), 371–421. https://doi.org/10.1016/j.pecs.2010.06.006.

(2) Edwards, T.; Maurice, L. Q. Surrogate Mixtures to Represent Complex Aviation and Rocket Fuels. *Journal of Propulsion and Power* **2001**, *17* (2), 461–466. https://doi.org/10.2514/2.5765.

(3) Pitz, W. J.; Mueller, C. J. Recent Progress in the Development of Diesel Surrogate Fuels. *Progress in Energy and Combustion Science* **2011**, *37* (3), 330–350. https://doi.org/10.1016/j.pecs.2010.06.004.

(4) Sarathy, S. M.; Farooq, A.; Kalghatgi, G. T. Recent Progress in Gasoline Surrogate Fuels. *Progress in Energy and Combustion Science* **2018**, *65*, 67–108. https://doi.org/10.1016/j.pecs.2017.09.004.

(5) Guibet, J.-C. *Fuels & Engines: Technology, Energy, Envionment - Volume 1*, Rev Ed.; 1999.

(6) Battin-Leclerc, F. Detailed Chemical Kinetic Models for the Low-Temperature Combustion of Hydrocarbons with Application to Gasoline and Diesel Fuel Surrogates. *Progress in Energy and Combustion Science* **2008**, *34* (4), 440–498. https://doi.org/10.1016/j.pecs.2007.10.002.

(7) Dryer, F. L. Chemical Kinetic and Combustion Characteristics of Transportation

Fuels. *Proceedings of the Combustion Institute* **2015**, *35* (1), 117–144. https://doi.org/10.1016/j.proci.2014.09.008.
(8) Zou, J.; Jin, H.; Liu, D.; Zhang, X.; Su, H.; Yang, J.; Farooq, A.; Li, Y. A Comprehensive Study on Low-Temperature Oxidation Chemistry of Cyclohexane. II. Experimental and Kinetic Modeling Investigation. *Combustion and Flame* **2021**, 111550. https://doi.org/10.1016/j.combustflame.2021.111550.
(9) Zou, J.; Li, Y.; Ye, L.; Jin, H. A Comprehensive Study on Low-Temperature Oxidation Chemistry of Cyclohexane. I. Conformational Analysis and Theoretical Study of First and Second Oxygen Addition. *Combustion and Flame* **2021**, 111658. https://doi.org/10.1016/j.combustflame.2021.111658.
(10) Serinyel, Z.; Herbinet, O.; Frottier, O.; Dirrenberger, P.; Warth, V.; Glaude, P. A.; Battin-Leclerc, F. An Experimental and Modeling Study of the Low- and High-Temperature Oxidation of Cyclohexane. *Combustion and Flame* **2013**, *160* (11), 2319–2332. https://doi.org/10.1016/j.combustflame.2013.05.016.
(11) Hemberger, P.; Bodi, A.; Bierkandt, T.; Köhler, M.; Kaczmarek, D.; Kasper, T. Photoelectron Photoion Coincidence Spectroscopy Provides Mechanistic Insights in Fuel Synthesis and Conversion. *Energy Fuels* **2021**, *35* (20), 16265–16302. https://doi.org/10.1021/acs.energyfuels.1c01712.
(12) Bourgalais, J.; Gouid, Z.; Herbinet, O.; Garcia, G. A.; Arnoux, P.; Wang, Z.; Tran, L.-S.; Vanhove, G.; Hochlaf, M.; Nahon, L. Isomer-Sensitive Characterization of Low Temperature Oxidation Reaction Products by Coupling a Jet-Stirred Reactor to an Electron/Ion Coincidence Spectrometer: Case of n-Pentane. *Physical Chemistry Chemical Physics* **2020**, *22* (3), 1222–1241.https://doi.org/10.1039/C9CP04992D.
(13) Bourgalais, J.; Herbinet, O.; Carstensen, H.-H.; Debleza, J.; Garcia, G. A.; Arnoux, P.; Tran, L. S.; Vanhove, G.; Liu, B.; Wang, Z.; Hochlaf, M.; Nahon, L.; Battin-Leclerc, F. Jet-Stirred Reactor Study of Low-Temperature Neopentane Oxidation: A Combined Theoretical, Chromatographic, Mass Spectrometric, and PEPICO Analysis. *Energy Fuels* **2021**, *35* (23), 19689–19704. https://doi.org/10.1021/acs.energyfuels.1c02080.
(14) Battin-Leclerc, F.; Bourgalais, J.; Gouid, Z.; Herbinet, O.; Garcia, G.; Arnoux, P.; Wang, Z.; Tran, L.-S.; Vanhove, G.; Nahon, L. Chemistry Deriving from OOQOOH Radicals in Alkane Low-Temperature Oxidation: A First Combined Theoretical and Electron-Ion Coincidence Mass Spectrometry Study. *Proceedings of the Combustion Institute* **2021**, *38* (1), 309–319. https://doi.org/10.1016/j.proci.2020.06.159.
(15) Tang, X.; Garcia, G. A.; Gil, J.-F.; Nahon, L. Vacuum Upgrade and Enhanced Performances of the Double Imaging Electron/Ion Coincidence End-Station at the Vacuum Ultraviolet Beamline DESIRS. *Review of Scientific Instruments* **2015**, *86* (12), 123108. https://doi.org/10.1063/1.4937624.
(16) Garcia, G. A.; Cunha de Miranda, B. K.; Tia, M.; Daly, S.; Nahon, L. DELICIOUS III: A Multipurpose Double Imaging Particle Coincidence Spectrometer for Gas Phase Vacuum Ultraviolet Photodynamics Studies. *Review of Scientific Instruments* **2013**, *84* (5), 053112. https://doi.org/10.1063/1.4807751.
(17) Pieper, J.; Schmitt, S.; Hemken, C.; Davies, E.; Wullenkord, J.; Brockhinke, A.; Krüger, J.; Garcia, G. A.; Nahon, L.; Lucassen, A.; Eisfeld, W.; Kohse-Höinghaus, K. Isomer Identification in Flames with Double-Imaging Photoelectron/Photoion Coincidence Spectroscopy (i^2PEPICO) Using Measured and Calculated Reference Photoelectron Spectra. *Zeitschrift für Physikalische Chemie* **2018**, *232* (2), 153–187. https://doi.org/10.1515/zpch-2017-1009.
(18) C. Poully, J.; P. Schermann, J.; Nieuwjaer, N.; Lecomte, F.; Grégoire, G.; Desfrançois, C.; A. Garcia, G.; Nahon, L.; Nandi, D.; Poisson, L.; Hochlaf, M. Photoionization of 2-Pyridone and 2-Hydroxypyridine. *Physical Chemistry Chemical Physics* **2010**, *12* (14), 3566–

3572. https://doi.org/10.1039/B923630A.
(19) Becke, A. D. Density-functional Thermochemistry. I. The Effect of the Exchange-only Gradient Correction. *J. Chem. Phys.* **1992**, *96* (3), 2155–2160. https://doi.org/10.1063/1.462066.
(20) Adamo, C.; Barone, V. Toward Reliable Density Functional Methods without Adjustable Parameters: The PBE0 Model. *J. Chem. Phys.* **1999**, *110* (13), 6158–6170. https://doi.org/10.1063/1.478522.
(21) Dunning, T. H. Gaussian Basis Sets for Use in Correlated Molecular Calculations. I. The Atoms Boron through Neon and Hydrogen. *J. Chem. Phys.* **1989**, *90* (2), 1007–1023. https://doi.org/10.1063/1.456153.
(22) Kendall, R. A.; Dunning, T. H.; Harrison, R. J. Electron Affinities of the First-row Atoms Revisited. Systematic Basis Sets and Wave Functions. *J. Chem. Phys.* **1992**, *96* (9), 6796–6806. https://doi.org/10.1063/1.462569.
(23) Bloino, J.; Biczysko, M.; Crescenzi, O.; Barone, V. Integrated Computational Approach to Vibrationally Resolved Electronic Spectra: Anisole as a Test Case. *J. Chem. Phys.* **2008**, *128* (24), 244105. https://doi.org/10.1063/1.2943140.
(24) Bloino, J.; Biczysko, M.; Santoro, F.; Barone, V. General Approach to Compute Vibrationally Resolved One-Photon Electronic Spectra. *J. Chem. Theory Comput*. **2010**, *6* (4), 1256-1274. https://pubs.acs.org/doi/10.1021/ct9006772.
(25) Bloino, J.; Baiardi, A.; Biczysko, M. Aiming at an accurate prediction of vibrational and electronic spectra for medium-to-large molecules: An overview. *International Journal of Quantum Chemistry*. **2016**, *116* (21), 1543-1574. https://onlinelibrary.wiley.com/doi/full/10.1002/qua.25188.
(26) Barone, V.; Bloino, J.; Biczysko, M.; Santoro, F. Fully Integrated Approach to Compute Vibrationally Resolved Optical Spectra: From Small Molecules to Macrosystems. *Journal of Chemical Theory and Computation*. **2009**, *5* (3), 540-554. https://pubs.acs.org/doi/10.1021/ct800474.
(27) Montgomery, J. A.; Frisch, M. J.; Ochterski, J. W.; Petersson, G. A. A Complete Basis Set Model Chemistry. VI. Use of Density Functional Geometries and Frequencies. *J. Chem. Phys.* **1999**, *110* (6), 2822–2827. https://doi.org/10.1063/1.477924.
(28) Montgomery, J. A.; Frisch, M. J.; Ochterski, J. W.; Petersson, G. A. A Complete Basis Set Model Chemistry. VII. Use of the Minimum Population Localization Method. *J. Chem. Phys.* **2000**, *112* (15), 6532–6542. https://doi.org/10.1063/1.481224.
(29) Adler, T. B.; Werner, H.-J.; Manby, F. R. Local Explicitly Correlated Second-Order Perturbation Theory for the Accurate Treatment of Large Molecules. *J. Chem. Phys.* **2009**, *130* (5), 054106. https://doi.org/10.1063/1.3040174.
(30) Adler, T. B.; Werner, H.-J. Local Explicitly Correlated Coupled-Cluster Methods: Efficient Removal of the Basis Set Incompleteness and Domain Errors. *J. Chem. Phys.* **2009**, *130* (24), 241101. https://doi.org/10.1063/1.3160675.
(31) Adler, T. B.; Knizia, G.; Werner, H.-J. A Simple and Efficient CCSD(T)-F12 Approximation. *J. Chem. Phys.* **2007**, *127* (22), 221106. https://doi.org/10.1063/1.2817618.
(32) Knizia, G.; Adler, T. B.; Werner, H.-J. Simplified CCSD(T)-F12 Methods: Theory and Benchmarks. *J. Chem. Phys.* **2009**, *130* (5), 054104. https://doi.org/10.1063/1.3054300.
(33) Yousaf, K. E.; Peterson, K. A. Optimized Auxiliary Basis Sets for Explicitly Correlated Methods. *J. Chem. Phys.* **2008**, *129* (18), 184108. https://doi.org/10.1063/1.3009271.
(34) Werner, H.-J.; Knowles, P. J.; Knizia, G.; Manby, F. R.; Schütz, M. Molpro: A General-Purpose Quantum Chemistry Program Package. *WIREs Computational Molecular Science* **2012**, *2* (2), 242–253. https://doi.org/10.1002/wcms.82.
(35) Cuoci, A.; Frassoldati, A.; Faravelli, T.; Ranzi, E. Numerical Modeling of Laminar

Flames with Detailed Kinetics Based on the Operator-Splitting Method. *Energy & Fuels* **2013**, *27* (12), 7730–7753. https://doi.org/10.1021/ef4016334.
(36) Cuoci, A.; Frassoldati, A.; Faravelli, T.; Ranzi, E. OpenSMOKE++: An Object-Oriented Framework for the Numerical Modeling of Reactive Systems with Detailed Kinetic Mechanisms. *Computer Physics Communications* **2015**, *192*, 237–264. https://doi.org/10.1016/j.cpc.2015.02.014.
(37) Zou, J.; Zhang, X.; Li, Y.; Ye, L.; Xing, L.; Li, W.; Cao, C.; Zhai, Y.; Qi, F.; Yang, J. Experimental and Kinetic Modeling Investigation on Ethylcyclohexane Low-Temperature Oxidation in a Jet-Stirred Reactor. *Combustion and Flame* **2020**, *214*, 211–223. https://doi.org/10.1016/j.combustflame.2019.12.038.
(38) Burke, S. M.; Metcalfe, W.; Herbinet, O.; Battin-Leclerc, F.; Haas, F. M.; Santner, J.; Dryer, F. L.; Curran, H. J. An Experimental and Modeling Study of Propene Oxidation. Part 1: Speciation Measurements in Jet-Stirred and Flow Reactors. *Combustion and Flame* **2014**, *161* (11), 2765–2784. https://doi.org/10.1016/j.combustflame.2014.05.010.
(39) Silke, E. J.; Pitz, W. J.; Westbrook, C. K.; Ribaucour, M. Detailed Chemical Kinetic Modeling of Cyclohexane Oxidation†. *J. Phys. Chem. A* **2007**, *111* (19), 3761–3775. https://doi.org/10.1021/jp067592d.
(40) Muller, C.; Michel, V.; Scacchi, G.; Côme, G. M. THERGAS: A Computer Program for the Evaluation of Thermochemical Data of Molecules and Free Radicals in the Gas Phase. *J. Chim. Phys.* **1995**, *92*, 1154–1178. https://doi.org/10.1051/jcp/1995921154.
(41) Ikuta, S.; Yoshihara, K.; Shiokawa, T.; Jinno, M.; Yokoyama, Y.; Ikeda, S. Photoelectron Spectroscopy of Cyclohexane, Cyclopentane, and Some Related Compounds. *Chem. Lett.* **1973**, *2* (12), 1237–1240. https://doi.org/10.1246/cl.1973.1237.
(42) Curran, H. J. Developing Detailed Chemical Kinetic Mechanisms for Fuel Combustion. *Proceedings of the Combustion Institute* **2019**, *37* (1), 57–81. https://doi.org/10.1016/j.proci.2018.06.054.
(43) Wang, Z.; Herbinet, O.; Hansen, N.; Battin-Leclerc, F. Exploring Hydroperoxides in Combustion: History, Recent Advances and Perspectives. *Progress in Energy and Combustion Science* **2019**, *73*, 132–181. https://doi.org/.10.1016/j.pecs.2019.02.003.
(44) Erman, P.; Karawajczyk, A.; Rachlew-Källne, E.; Strömholm, C.; Larsson, J.; Persson, A.; Zerne, R. Direct Determination of the Ionization Potential of CO by Resonantly Enhanced Multiphoton Ionization Mass Spectroscopy. *Chemical Physics Letters* **1993**, *215* (1), 173–178. https://doi.org/10.1016/0009-2614(93)89283-N.
(45) Battin-Leclerc, F.; Herbinet, O.; Glaude, P.-A.; Fournet, R.; Zhou, Z.; Deng, L.; Guo, H.; Xie, M.; Qi, F. New Experimental Evidences about the Formation and Consumption of Ketohydroperoxides. *Proceedings of the Combustion Institute* **2011**, *33* (1), 325–331. https://doi.org/10.1016/j.proci.2010.05.001.
(46) Kimura, K. *Handbook of HeI Photoelectron Spectra of Fundamental Organic Molecules*; Halsted Press, 1981.
(47) Bourgalais, J.; Jiang, Z.; Bloino, J.; Herbinet, O.; Carstensen, H.-H.; Garcia, G. A.; Arnoux, P.; Tran, L.-S.; Vanhove, G.; Nahon, L.; Battin-Leclerc, F.; Hochlaf, M. Accounting for Molecular Flexibility in Photoionization: Case of *tert*-butyl Hydroperoxide. *Phys. Chem. Chem. Phys.* **2022**, *24* (18), 10826-10837. https://doi.org/10.1039/D2CP00929C.
(48) Sheps, L.; Dewyer, A. L.; Demireva, M.; Zádor, J. Quantitative Detection of Products and Radical Intermediates in Low-Temperature Oxidation of Cyclopentane. *J. Phys. Chem. A* **2021**, *125* (20), 4467–4479. https://doi.org/10.1021/acs.jpca.1c02001.
(49) Tian, S. X.; Kishimoto, N.; Ohno, K. Electronic Structures of 1-Adamantanol, Cyclohexanol and Cyclohexanone and Anisotropic Interactions with He*(2^3S) Atoms: Collision-Energy-Resolved Penning Ionization Electron Spectroscopy Combined with Quantum Chemistry Calculations. *Journal of Electron Spectroscopy and Related Phenomena*

2002, *127* (3), 167–181. https://doi.org/10.1016/S0368-2048(02)00186-X.
(50) Yang, B.; Wang, J.; Cool, T. A.; Hansen, N.; Skeen, S.; Osborn, D. L. Absolute Photoionization Cross-Sections of Some Combustion Intermediates. *International Journal of Mass Spectrometry* **2012**, *309*, 118–128. https://doi.org/10.1016/j.ijms.2011.09.006.
(51) Person, J. C.; Nicole, P. P. Isotope Effects in the Photoionization Yields and the Absorption Cross Sections for Acetylene, Propyne, and Propene. *J. Chem. Phys.* **1970**, *53* (5), 1767–1774. https://doi.org/10.1063/1.1674254.
(52) Jalan, A.; Alecu, I. M.; Meana-Pañeda, R.; Aguilera-Iparraguirre, J.; Yang, K. R.; Merchant, S. S.; Truhlar, D. G.; Green, W. H. New Pathways for Formation of Acids and Carbonyl Products in Low-Temperature Oxidation: The Korcek Decomposition of γ-Ketohydroperoxides. *Journal of the American Chemical Society* **2013**, *135* (30), 11100–11114. https://doi.org/10.1021/ja4034439.
(53) Wang, Z.; Zhang, L.; Moshammer, K.; Popolan-Vaida, D. M.; Shankar, V. S. B.; Lucassen, A.; Hemken, C.; Taatjes, C. A.; Leone, S. R.; Kohse-Höinghaus, K.; Hansen, N.; Dagaut, P.; Sarathy, S. M. Additional Chain-Branching Pathways in the Low-Temperature Oxidation of Branched Alkanes. *Combustion and Flame* **2016**, *164*, 386–396. https://doi.org/10.1016/j.combustflame.2015.11.035.
(54) Wang, Z.; Popolan-Vaida, D. M.; Chen, B.; Moshammer, K.; Mohamed, S. Y.; Wang, H.; Sioud, S.; Raji, M. A.; Kohse-Höinghaus, K.; Hansen, N.; Dagaut, P.; Leone, S. R.; Sarathy, S. M. Unraveling the Structure and Chemical Mechanisms of Highly Oxygenated Intermediates in Oxidation of Organic Compounds. *Proceedings of the National Academy of Sciences* **2017**, *114* (50), 13102–13107. https://doi.org/10.1073/pnas.1707564114.
(55) Knepp, A. M.; Meloni, G.; Jusinski, L. E.; Taatjes, C. A.; Cavallotti, C.; Klippenstein, S. J. Theory, Measurements, and Modeling of OH and HO2 Formation in the Reaction of Cyclohexyl Radicals with O2. *Phys. Chem. Chem. Phys.* **2007**, *9* (31), 4315–4331. https://doi.org/10.1039/B705934E.